THE JOURNAL OF PHYSICAL CHEMISTRY C

Article

pubs.acs.org/JPCC

Insight into the Reduction of NO by H_2 on the Stepped Pd(211) Surface

Lixia Ling,[†] Zhongbei Zhao,[†] Xue Feng,[†] Qiang Wang,[‡] Baojun Wang,[*,§] Riguang Zhang,[§] and Debao Li[‡]

[†]College of Chemistry and Chemical Engineering, Taiyuan University of Technology, Taiyuan 030024, Shanxi, People's Republic of China

[‡]State Key Laboratory of Coal Conversion, Institute of Coal Chemistry, Chinese Academy of Sciences, Taiyuan 030001, Shanxi, People's Republic of China

[§]Key Laboratory of Coal Science and Technology, Taiyuan University of Technology, Ministry of Education and Shanxi Province, Taiyuan 030024, Shanxi, People's Republic of China

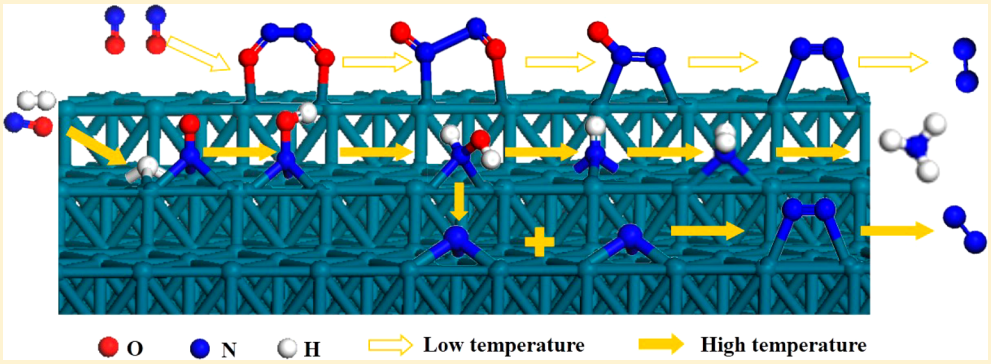

ABSTRACT: A periodic density functional theory (DFT) calculation has been used to study the NO reduction by H_2 on the stepped Pd(211) surface. The main route of N_2 generation changes with temperature increasing. The dimer path is main for the formation of N_2 at low temperature, in which two NO react and generate N_2O_2, and then N_2O_2 decompose to produce N_2. However, the active N path becomes main to generate N_2 via NO hydrogenate and dissociate to produce active N at high temperature. The formation of NH_3 is via the successive hydrogenation of N or NH. Additionally, energy barriers showed that the Pd(211) surface exhibited higher catalytic activity to the reduction of NO by H_2 than that on the Pd(111) surface, and the kinetics showed that the selectivity of N_2 is higher than that of NH_3 on the stepped Pd(211) surface below about 500 K.

1. INTRODUCTION

Atmospheric NO has attracted attention over the past decades due to environmental problems including toxic smog and acid rain,[1−3] which are mainly produced from industrial and automotive exhausts. Currently, NO in flue gas is mainly controlled by high-temperature selective catalytic reduction (SCR) with ammonia (NH_3), which is commercialized to remove NO from coal-fired power plants for many years.[4−9] Nevertheless, many problems exist in the NH_3−SCR reaction, such as Vanadium catalyst emissions, unreacted ammonia slipping, equipment fouling that caused by "white powder" and high running costs.[10,11] Compared with the NH_3−SCR, the selective catalytic reduction with hydrogen (H_2−SCR) is highly promising but still under the development process. Hydrogen has been reported to be active reducing agent for the NO/H_2 reaction and has the potential application to reduce NO emissions from stationary sources.[12,13]

Different catalysts are explored with regard to the decomposition and reduction of NO, including Cu-ZSM5,[14,15] Pd−H-ZSM5,[16] Fe-ZSM5[17] and noble metals[18−20] in which, noble metals attract more attention due to their activity or selectivity for the reduction of NO.[12] The decomposition and reduction of NO on different noble metal surfaces were researched, and the results indicate that the barrier for the dissociation of NO decreases in the order of Pt(111) > Rh(111) > Ru(001) > Re(001) and the barrier for N_2 formation increases in the reverse order of Pt < Rh < Ru < Re.[21] Huai et al.[22] studied the NO reduction mechanism by H_2 on the Pt(100) surface and subsurface modified with oxygen atoms, N_2 was the main product via the reaction of N+N → N_2, the selectivity of which is larger than 90%. However, N_2O was the main product via the intermediate of NHOH at low temperatures on the Pt(111) surface by the density functional theory (DFT) study.[23] The reduction of NO by H_2 on Pt/Al_2O_3 by theoretical and experimental methods has also been studied, and the results showed that NO prefers to react with H to form NHOH prior to

Received: May 24, 2017
Revised: July 10, 2017
Published: July 11, 2017

DOI: 10.1021/acs.jpcc.7b05024
J. Phys. Chem. C 2017, 121, 16399−16414

N−O bond activation in the presence of H_2, and N_2O is formed via the dimer reaction in the absence of H_2.[24] The dimer reaction pathway during NO reduction has also been investigated on the Au(111) surface, and leads to the formation of N_2O.[25] The same reaction was investigated on Rh(111) and Rh(221) surfaces, and high N_2 selectivity is obtained.[26] It can be seen that the products are different for the same reduction process on different catalysts, even on the different surfaces of the same catalyst. Pd-based catalysts have received much more attention due to high low-temperature activity and relative low price. The kinetic measurement by steady-state experiment shows that Pd is significantly highly active for the NO/H_2 reaction but much less selective, while the opposite trend characterizes for Rh.[27] NO could be completely reduced over Pd/Al_2O_3 and Pt/Al_2O_3 in the range of 423−623 K when H_2 was used as the reducing agent, and Pd/Al_2O_3 presented higher NO reduction activity in the CO−H_2 reducing condition than that of Pt/Al_2O_3.[28] In addition, lower formation of NH_3 on Pd/$LaCoO_3$ than that on Pt/$LaCoO_3$ is attributed to competitive adsorption more in favor of H on Pt/$LaCoO_3$.[29] The reduction of NO by H_2 on the Pd(111) has also been studied by the DFT method, and the microkinetic analysis showed that N_2O is a major product at low temperature while N_2 becomes dominant with the temperature increasing.[30]

The catalytic activity and product selectivity are greatly dependent on the surface structure. The reduction of NO by H_2 on Rh(111) and Rh(221) surfaces showed that the reduction of NO on the stepped Rh(221) surface was easier than that on the flat Rh(111) surface, and energy barriers of decomposition of NO on the Rh(221) surface with and without H were same. For the selectivity of products, N_2O is the dominant product at low temperature on the Rh(221) surface, and N_2 becomes the main product above 480 K, while NH_3 is the main product on the Rh(111) surface under near practical condition.[26] The adsorption, dissociation, and desorption of NO on Pd(111), (100), and (311) surfaces indicated that the stepped Pd(311) surface was active for the thermal dissociation of NO due to the formation of N_2 and N_2O, while NO molecule desorbed from Pd(111) and Pd(100) surfaces.[31] In addition, N_2O easily dissociated on the Pd(211) surface leading to the emission of N_2 in a steady-state NO+CO+D_2 reaction,[32] while N_2O is as the product desorbing from the Pd(111) surface.[33] The experiment shows that the catalytic activity of Pd(211) for the reaction of NO-H_2 depends on the ratio of the area between the (100) steps and the (111) terraces[34] and the stepped Pd(21l) surface is more active for NO decomposition than the Pd(1ll) surface.[35,36] The DFT results also demonstrate that the dissociation of NO on Pd(211) is facilitated compared to that on Pd(111).[37] However, the catalytic activity of Pd(211) for the reduction of NO by H_2 is unclear.

In this work, adsorptions of all possible species during the reduction of NO by H_2 on the stepped Pd(211) surface have been studied. Then, the dissociation of NO and correlated reactions are investigated to obtain the favorable path for the formation of active N and NH. Further, the formation pathways of all possible products, including N_2, NH_3 and H_2O, are explored. Moreover, the results are expected to obtain the selectivity of main N-containing products and the favorable reaction path on the Pd(211) surface. In addition, the effect of the stepped Pd(211) surface on the reduction of NO will be obtained compared with the flat Pd(111) surface.

2. COMPUTATIONAL DETAILS

2.1. Surface Models. The stepped Pd(211) surface has been investigated by XRD spectra when Pd was loaded on C, SnO_2/C and SnO_2/multiwalled carbon nanotubes (MWCNTs),[38,39] which was also built as a catalytic surface to study the adsorption and reaction of gases in theory.[40,41] Therefore, the Pd(211) surface is modeled using a $p(1 \times 3)$ surface unit cell[42] with four layers in the z-direction, and a vacuum thickness of 12 Å is employed to avoid interactions between slabs. It is a common method to deal with the interaction and reactions between gases and solid modeling by the slab, which is widely used in the different gases adsorption and reactions on the Pd(211) surface,[43,44] as well as the activation of NO and reduction by H_2.[45,24] The bottom two layers are kept frozen to their optimized bulk positions, while the others were allowed to relax. The isolated molecules and atoms are optimized in a large cell of 10 × 10 × 10 Å. Five types of sites on the step Pd(211) surface, involving top (T), bridge (B), 4-fold hollow site (H_O), 3-fold hollow fcc (F), and hcp (H) sites, are examined. They are 14 different adsorption sites, in which T1 and B1 are at the step edge; T2 and B4 are at the lower edge; T3, B2, B3, B6, H1, H2, F1, and F2 are on the (111) terrace; B5 and H_O are on the (100) step, as shown in Figure 1a,b.

2.2. Calculation Methods. We used the Vienna *ab* initio simulation package (VASP)[46] for all calculations. To deal with the exchange−correlation energies, the generalized gradient approximation (GGA) with the function of Perdew−Burke−Ernzerhof (PBE)[47] was carried out. The projector-augmented wave (PAW)[48,49] method was implemented to describe the interaction between ionic cores and valence electrons. A plane-wave basis set with an energy cutoff of 400 eV was chosen to

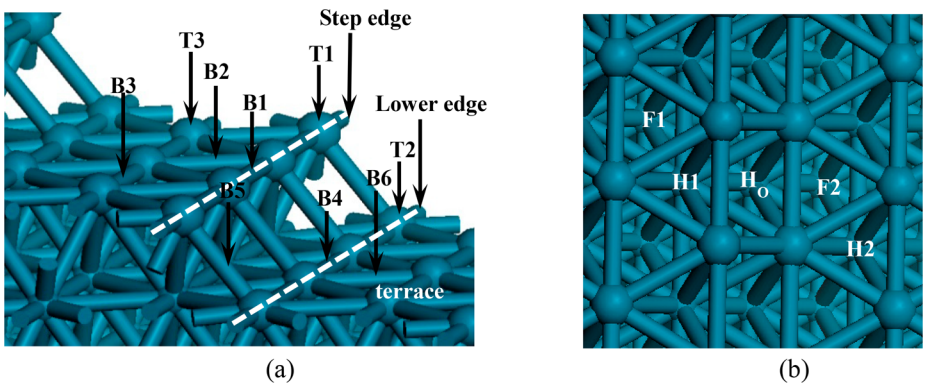

Figure 1. Optimized slab model of Pd(211): (a) side view; (b) top view.

DOI: 10.1021/acs.jpcc.7b05024
J. Phys. Chem. C 2017, 121, 16399−16414

expand the one-electron wave function,[50,51] and the integration of the Brillouim zone was conducted using (4 × 3 × 1) Monkhorst−Pack grids for surface. In addition, optimization was carried out by calculating partial occupancies of the wave function using Methfessel-Paxton method with a width of 0.1 eV. The criterion for convergence of the electronic energy and force were less than 5×10^{-6} eV and 0.01 eV·Å^{-1}, respectively.

The climbing-image nudged elastic band (CI-NEB) method combining with the dimer method was employed to determine the transition state of each elementary reaction step.[52,53] CI-NEB was used to locate the possible structural images between reactant and product with the coarser convergence criterion (electronic energy: 1×10^{-4} eV; force: 0.3 eV·Å^{-1}). Furthermore, the image close to the transition structure was then optimized using the dimer method to electronic energy of 1×10^{-7} eV and force of 0.05 eV·Å^{-1}. This combination method was widely used in other studies due to its high calculation efficiency.[54−56]

Four intermediate images were interpolated between reactant and product states for each elementary step in this study. In order to test the accuracy, eight intermediate images using CI-NEB together with the dimer method was employed to search the transition state for the reaction: NOH+H → NH+OH. Transition states and the corresponding energy barriers with different image numbers are shown in Table 1. It can be seen that transition states and activation energies are nearly same with different intermediate images. It can be concluded that four images is sufficient for the search of transition states, which was also used in other work.[57−59]

Additionally, a smearing value of 0.2 eV was used to accelerate the convergence. The transition state for the dissociation of *trans*-N_2O_2 into N_2O and O was also searched using the same parameters as the optimization (electronic energy: 5×10^{-6} eV; force: 0.01 eV·Å^{-1}; smearing: 0.1 eV), and the energy difference is only 1.0 kJ·mol^{-1} by using those two parameters.

The activation barrier E_a is defined as the total energy difference between the transition state and the corresponding initial stable structure, as Equation 1:

$$E_a = E_{TS} - E_R + \Delta E_{ZPE} \quad (1)$$

The adsorption energy, E_{ads}, on the Pd(211) surface is defined by using eq 2:

$$E_{ads} = E_{slab\text{-}adsorbate} - (E_{slab} + E_{adsorbate}) \quad (2)$$

where $E_{slab\text{-}adsorbate}$ is the total energy of the Pd(211) slab and adsorbates system in its equilibrium state; E_{slab} is the energy of the Pd(211) surface, and $E_{adsorbate}$ is the energy of the isolated adsorbates.

The stepwise NO adsorption energies ($\Delta E_{ads}'$) have been defined to determine the adsorption saturation of NO on the Pd(211) surface, according to eq 3:

$$\Delta E_{ads}' = E_{NOn+1/slab} - (E_{NOn/slab} + E_{NO}) \quad (3)$$

where $\Delta E_{ads}'$ refers to the energy change between the adsorbed (n+1)NO systems and the adsorbed nNO systems plus the gaseous NO molecule. A positive $\Delta E_{ads}'$ for n+1 adsorbed NO molecules indicates the adsorption saturation with nNO molecules.

3. RESULTS AND DISCUSSION

3.1. Adsorptions of Surface Species. Adsorptions of reactants, possible intermediates and products on the stepped Pd(211) surface are investigated, and 14 adsorption sites are considered. Most adsorption configurations, the corresponding adsorption energies, and some important geometric parameters are shown in Figure 2 and Table 2.

3.1.1. Adsorption of N_xO_y (x, y = 0−2). N atom is more likely to adsorb at H1 site on the (111) terrace and the adsorption energy is −464.9 kJ·mol^{-1}. However, both F1 and H1 are the most stable adsorption sites for the adsorption of O atom with adsorption energies of −451.6 and −447.0 kJ·mol^{-1}.

For the adsorption of NO, it prefers to adsorb at H1 site on the (111) terrace and bridge site (B1) at the step edge, which are consistent with previous work that NO is more easily adsorbed on the (111) terrace of the stepped Pd(112) surface.[60] The adsorbed NO molecule is binding with nitrogen end down to the surface and N−O bond lengths are 1.212 and 1.197 Å. The result is consistent with the previous work, in which the N−O bond length is 1.180 Å.[45] Two adsorption energies are similar to −222.1 and −218.4 kJ·mol^{-1}, which are consistent with previous work (−225.8 kJ·mol^{-1}).[61]

N_2 parallelly adsorbs at the step edge bridge site with an adsorption energy of −47.2 kJ·mol^{-1}.

There are two stable adsorption sites for N_2O. One is that N_2O molecule binds with the Pd atom at the step edge top site through its terminal N (N_2O_{T1}), which is a nearly linear geometry with an adsorption energy of −32.0 kJ·mol^{-1}. The length of N−N and N−O are 1.152 and 1.201 Å, respectively. Other one is that N_2O molecule is connected to the surface via two N, and the O−N−N is with an angle of 137.70° in the N_2O_{B1} configuration. An energy released from the adsorption process is −25.4 kJ·mol^{-1} and the distance of N−N and N−O are 1.228 and 1.242 Å.

Table 1. Transition State Structures and the Corresponding Activation Energies of NOH+H → NH+OH with Different Image Numbers

Method	Image numbers	Energy barrier (kJ·mol^{-1})	NOH+H(a)	TS	NH+OH
Cl-NEB + dimer	4	87.3	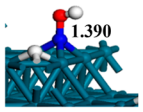	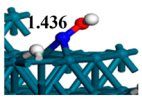	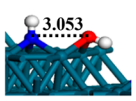
Cl-NEB+ dimer	8	90.0	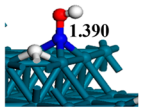	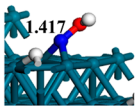	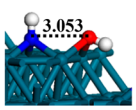

DOI: 10.1021/acs.jpcc.7b05024
J. Phys. Chem. C 2017, 121, 16399−16414

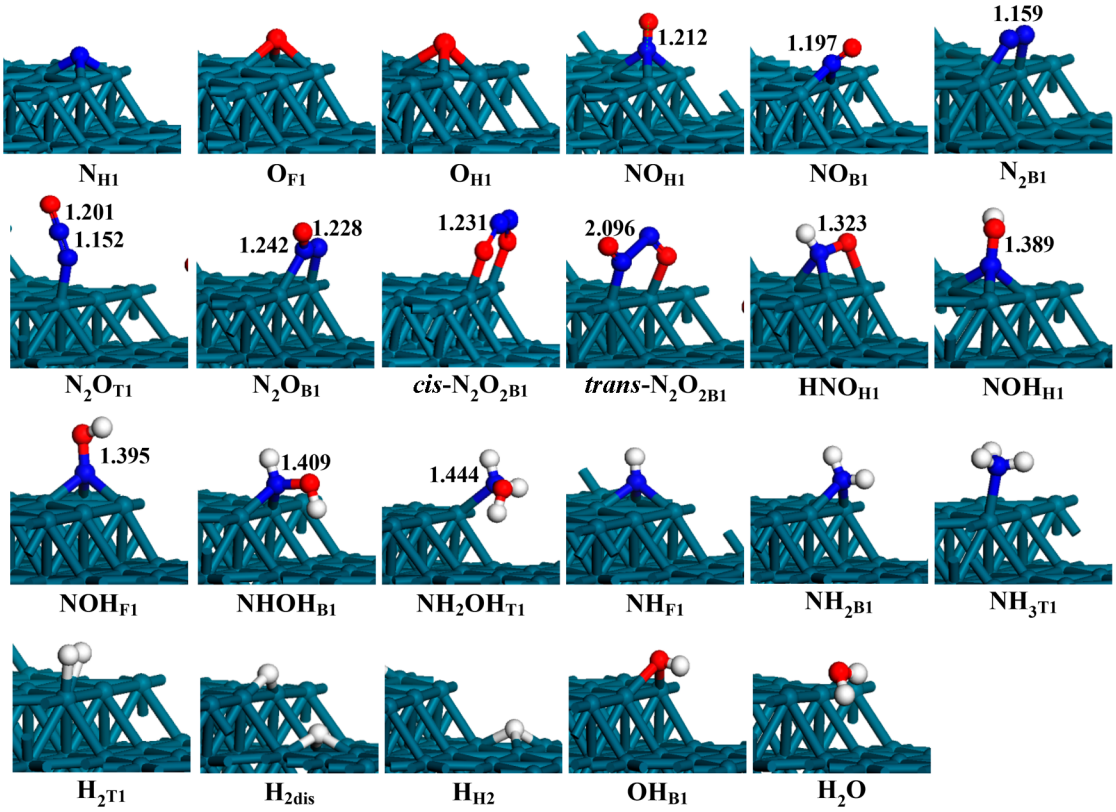

Figure 2. Stable adsorption configurations of possible species involved in the reduction of NO by H_2 on the stepped Pd(211) surface. Bond lengths are in angstroms.

Table 2. Adsorption Energies of Reaction Species on the Stepped Pd(211) Surface

adsorption species	E_{ads} (kJ·mol^{-1})	adsorption species	E_{ads} (kJ·mol^{-1})
N_{H1}	−464.9	NH_{F1}	−370.5
O_{F1}; O_{H1}	−451.6; −447.0	NH_{2B1}	−270.0
NO_{H1}; NO_{B1}	−222.1; −218.4	NH_{3T1}	−79.7
N_{2B1}	−47.2	H_{2T1}	−38.4
N_2O_{T1}; N_2O_{B1}	−32.0; −25.4	H_{2dis}	−92.4
cis-N_2O_{2B1}	−132.3	H_{H2}	−268.4
trans-N_2O_{2B1}	−143.3	OH_{B1}	−300.1
HNO_{H1}	−177.9	H_2O	−37.9
NOH_{H1}; NOH_{F1}	−265.5; −263.7		
$NHOH_{B1}$	−219.7		
NH_2OH_{T1}	−102.9		

Both *cis*-N_2O_2[62] and *trans*-N_2O_2 exit on Pd(111),[63] as well as Au(111),[25] Ag(111),[64] Cu(100) and (111),[65,66] silicon (Si)-doped graphene,[67] and BaO (100) surface[68] via two N atoms connecting to each other. The *cis*-N_2O_2 adsorbs at the step edge bridge site via two O atoms, while one N atom and one O atom bind to surface Pd atoms at the B1 site for the adsorption of *trans*-N_2O_2. In the adsorption configuration of *cis*-N_2O_2, the bond length of N−N is 1.231 Å with an adsorption energy of −132.3 kJ·mol^{-1}. For the adsorbed *trans*-N_2O_2, the bond length of N−N (2.096 Å) is slightly longer than that in the gas phase with 1.943 Å,[30] which shows that it is activated. The adsorption energy is −143.3 kJ·mol^{-1}.

3.1.2. Adsorption of HNO, NOH, NHOH, and NH_2OH. In the reduction process of NO by H_2, HNO, NOH, NHOH, and NH_2OH are possible intermediates.[23] The stable adsorption configurations are obtained, as shown in Figure 2. HNO prefers to adsorb at hcp site on the (111) terrace, which is the same as that on the Rh(221) surface through N and O adsorbing at the hcp site.[26] The bond length of N−O in HNO is 1.323 Å, the angle of H−N−O is 101.19°, and the adsorption energy is −177.9 kJ·mol^{-1}. NOH is found to adsorb at the 3-fold-coordinated hollow sites via N atom binding to three Pd atoms. The similar adsorption energies of −265.5 and −263.7 kJ·mol^{-1} are gotten for adsorptions at H1 and F1 sites on the (111) terrace. NHOH is located at the step edge bridge site via N atom binding to Pd−Pd bond, shown as $NHOH_{B1}$ with an adsorption energy of −219.7 kJ·mol^{-1}. As for the adsorption of NH_2OH, its most stable adsorption position is at the T1 site, where N atom connects to Pd atom at the step edge. The distance of N−O of NH_2OH is 1.444 Å and the adsorption energy is −102.9 kJ·mol^{-1}.

3.1.3. Adsorption of N_xH_y (x = 0−1, y = 1−3), OH and H_2O. During the reduction of NO by H_2, the dissociated N may combine with the surface H leading to the formation of NH, NH_2 and NH_3 species. The most stable adsorption sites for NH, NH_2, and NH_3 are F1, B1, and T1, respectively. Comparing with the strong chemical adsorption of NH and NH_2 with adsorption energies of −370.5 and −270.0 kJ·mol^{-1}, the adsorption of NH_3 is a weak chemical adsorption with an adsorption energy of −79.7 kJ·mol^{-1}. It can be seen that adsorbed NH and NH_2 are two stable intermediates, which are also investigated in the reduction of NO on the Pd(111) surface[30] and Pt(111) surface.[23]

H_2 adsorbs on the surface with molecule and dissociated modes, the molecular one is at the top site and parallel to the surface (H_{2T1}), and the adsorption energy is only −38.4 kJ·mol^{-1}. When it is placed at F2 on the (111) terrace, H_2 is dissociated without an energy barrier. The adsorption energy of −92.4 kJ·mol^{-1} shows that H is easily formed. The same process was observed on the Rh(221) surface.[26] H prefers to adsorb

DOI: 10.1021/acs.jpcc.7b05024
J. Phys. Chem. C 2017, 121, 16399−16414

at H2, H1, F1, F2, and B1 site with similar adsorption energies, which are −268.4, −268.0, −267.0, −266.6, and −265.4 kJ·mol^{-1}, respectively. Only the configuration of H on the (111) terrace is shown as H_{H2} in Figure 2. These results are in agreement with the previous work, in which the adsorption energy of H is −269.2 kJ·mol^{-1}.[69]

OH tends to adsorb at the B1 site through O atom with an adsorption energy of −300.1 kJ·mol^{-1}. The adsorption of H_2O is very weak with a little adsorption energy of −37.9 kJ·mol^{-1}, which is in favor of the desorption.

3.2. Decomposition of NO and Correlated Further Reactions. For the decomposition of NO, the coverage of NO on the stepped Pd(211) surface is first investigated. On one hand, the stable (111) terrace and bridge sites at the step edge are first considered as the adsorption sites. Additionally, the stepwise NO adsorption energies and the corresponding structures on the Pd(211) surface are shown in Table 3. It can be seen that it is unfavorable for the adsorption of the eighth NO molecule, and two NO molecules are repelled to leave the surface when eight NO molecules are on the stable sites on the Pd(211) surface. In agreement with the adsorption of CO on the Ni(100) surface, the adsorption mode changes with the adsorbed CO increasing, and the saturated coverage is 9/12 ML.[70]

Moreover, the concentration of NO is very low, and just 500 ppm of NO (on a volume basis) in the gas stream was inlet into the reactor in a small laboratory.[71−73] So the active site on the catalyst surface cannot be fully covered by NO.

Thus the reduction of NO by H_2 proceeds at the low coverage.

3.2.1. NO Dissociation and Hydrogenation Reaction. The dissociation of NO is the first step in the reduction of NO by H_2.[74] In addition, hydrogenation of NO can also occur and some intermediates are investigated. Therefore, four possible reactions about the dissociation and hydrogenation of NO are considered on the Pd(211) surface, including:

Step 1 $NO \rightarrow N + O$

Step 2 $NO + H \rightarrow N + OH$

Step 3 $NO + H \rightarrow HNO$

Step 4 $NO + H \rightarrow NOH$

NO direct dissociation starts from the most stable H1 adsorption site on the (111) terrace, and formed N and O are at H1 sites. An energy barrier of 288.4 kJ·mol^{-1} is needed for this step via TS1, indicating that the direct dissociation of NO on the Pd(211) surface is hard. On the Pd(111) surface, an energy barrier of 227.7 kJ·mol^{-1} is needed for the direct step starting from NO_{hcp}*,[30] showing that both Pd(111) and Pd(211) surfaces are not in favor of the direct dissociation of NO. However, the stepped Rh(221) surface is likely more favorable than that of Rh(111) surface for NO direct decomposition.[26] H-assisted dissociation elementary step for NO is also considered due to high energy barrier for the NO direct dissociation. NO is at the stable H1 site, H is on the adjacent (111) terrace with NO in NO+H(a). Relatively high energy barrier of 269.2 kJ·mol^{-1} for NO+H→N+OH is obtained, indicating that this is not likely to occur on the Pd(211) surface. It was certified that this step is an elementary reaction via interpolating eight intermediate images between reactant and product states, and the transition state and the corresponding energy barrier are shown as TS2′ in Figure 3. This elementary reaction step was also investigated on the Rh(111) and Rh(221) surfaces with lower energy barriers than that on the Pd(211) surface.[26] H-assisted dissociation was also investigated for the cleavage of C−O bond in CO molecule, the reaction rates for elementary step (CO+H→C+OH) at different temperatures on the Ni(211)

Table 3. Stepwise NO Adsorption Energies and the Corresponding Structures on the Pd(211) Surface

Molecular number	$\Delta E_{ads}'$ (kJ·mol^{-1})	Adsorption configurations	Molecular number	$\Delta E_{ads}'$ (kJ·mol^{-1})	Adsorption configurations
1	-222.1	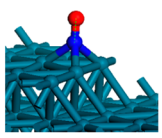	5	-171.3	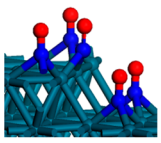
2	-196.7	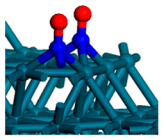	6	-102.9	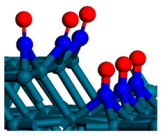
3	-124.1	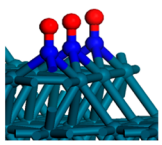	7	-0.24	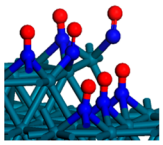
4	-135.4	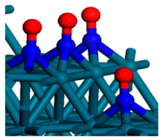	8	5.0	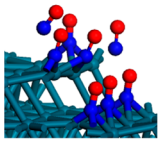

DOI: 10.1021/acs.jpcc.7b05024
J. Phys. Chem. C 2017, 121, 16399−16414

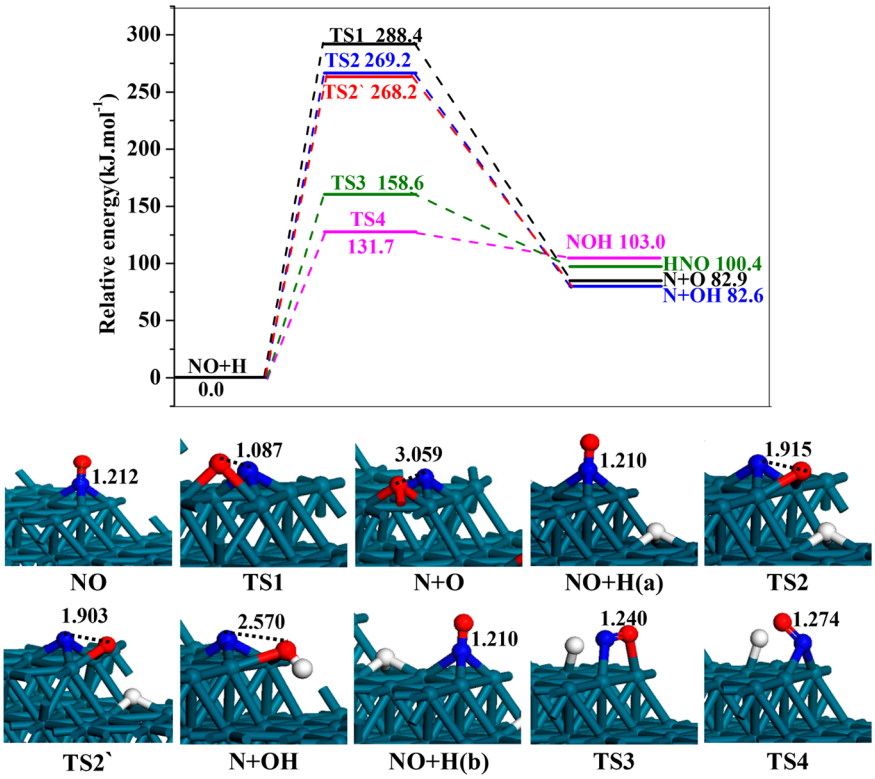

Figure 3. Potential energy diagram of the NO dissociation and hydrogenation including ZPE correction, and corresponding configurations of initial states, transition states, and final states. Bond lengths are in angstroms.

surface were obtained.[75] They are two elementary steps for hydrogenation of NO via H attracting to N and O in NO starting from NO+H(b), in which H is at F1 site on the same (111) terrace with NO, HNO and NOH intermediates are formed via TS3 and TS4 by overcoming energy barriers of 158.6 and 131.7 kJ·mol^{-1}. Comparing with energies barriers for all four elementary steps for the reaction of NO, NO hydrogenation forming NOH intermediate is more favorable than other three steps. However, H-assisted dissociation reactions are main on the Pd/Al_2O_3[76] and Pd(111) surface,[30] and NO direct dissociation steps are more likely to occur on Rh(111) and Rh(221) surfaces[26] leading to the formation of active N. Therefore, the correlated further reactions of NOH are discussed in the following sections.

3.2.2. Correlated Reactions of NOH. There are four possible further reactions for NOH, the direct dissociation step (NOH→N+OH), H-assisted dissociation steps (NOH+H→NH+OH and NOH+H→N+H_2O), as well as the hydrogenation step (NOH+H→NHOH) are investigated, as shown in Steps 5−8. The potential energy diagram for the reaction of NOH, and the corresponding configurations are shown in Figure 4.

The direct dissociation of NOH leads to the formation of N and OH is first considered. The N−O bond is cleaved via TS5, and an energy barrier of 71.1 kJ·mol^{-1} is needed to be overcome. For the H-assisted dissociation reaction of HNO, two elementary steps are investigated. When H and NOH coadsorb on the same (111) terrace [NOH+H(a)], it needs to overcome an energy barrier of 87.3 kJ·mol^{-1} in the process of H atom attacking to N of NOH to form NH and OH, and the elementary reaction is exothermic by −103.8 kJ·mol^{-1}. This step is also verified to be an elementary step via interpolating eight intermediate images between reactant and product states, the transition state and energy barriers can be seen in Table 1. The same elementary step

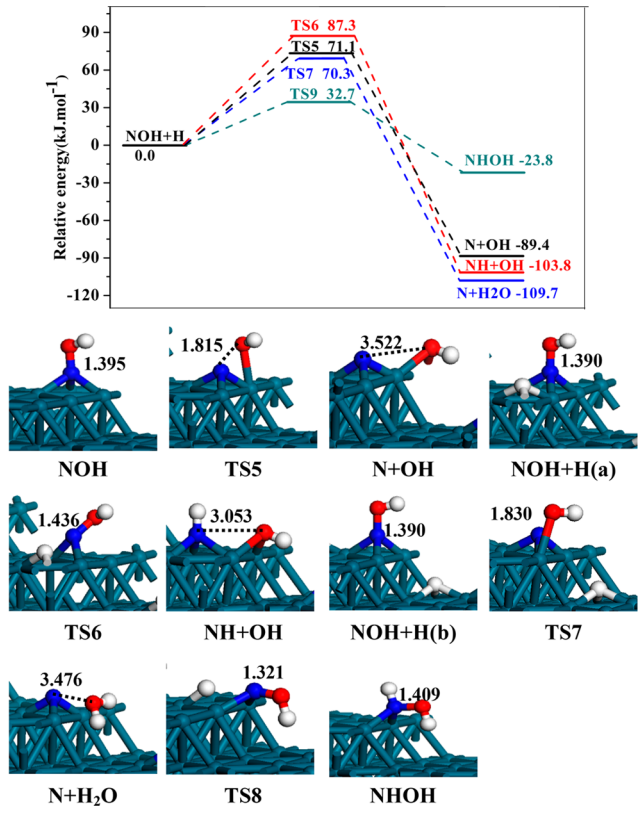

Figure 4. Potential energy diagram of correlated reactions of NOH including ZPE correction together with corresponding configurations of initial states, transition states, and final states. Bond lengths are in angstroms.

DOI: 10.1021/acs.jpcc.7b05024
J. Phys. Chem. C 2017, 121, 16399−16414

was also investigated on the Pd(111) surface with an energy barrier of 119.6 kJ·mol^{-1},[30] which is higher that on the stepped Pd(211) surface. For the process of H attacking to O of NOH leading to the formation of H_2O and N starting from H and NOH on the adjacent (111) terrace, the activation barrier is 70.3 kJ·mol^{-1}. A little activation barrier of 32.7 kJ·mol^{-1} is needed for the hydrogenation reaction, in which NOH+H(a) is the initial structure, and H fuses with NOH through N producing NHOH. It can be seen that the directed reaction and H-assisted dissociation reactions of NOH are difficult to occur due to high energy barriers, the same results are also obtained on the Pd(111) surface.[30] In addition, the elementary step (NOH+H→NHOH) is more favorable than other three elementary steps, and NHOH is an important intermediate. This intermediate is also investigated on the Pt(111) surface and as the main source of N by the further dissociation.[23,24]

Step 5 $NOH \rightarrow N + OH$

Step 6 $NOH + H \rightarrow NH + OH$

Step 7 $NOH + H \rightarrow N + H_2O$

Step 8 $NOH + H \rightarrow NHOH$

3.2.3. Correlated Reactions of NHOH. We discuss four possible related reactions for NHOH, which are shown as below:

Step 9 $NHOH \rightarrow NH + OH$

Step 10 $NHOH + H \rightarrow N + H_2O$

Step 11 $NHOH + H \rightarrow NH + H_2O$

Step 12 $NHOH + H \rightarrow NH_2OH$

The cleavage of N−O bond in NHOH leads to the formation of NH and OH, which are located at H1 site and B1 sites, respectively. The activation energy is 109.0 kJ·mol^{-1}, and the reaction is exothermic with a reaction energy of −79.2 kJ·mol^{-1}. This process is similar to that on the Pt(111) surface with an energy barrier of 67.5 kJ·mol^{-1} and an reaction energy of −80.1 kJ·mol^{-1} at low coverage.[23] The other direct dissociation reaction is that H of NHOH transfers from N to O, and H_2O is formed accompanying with the cleavage of N−H. This elementary step is exothermic with a reaction energy of −87.0 kJ·mol^{-1} and the activation energy barrier is 105.8 kJ·mol^{-1}. There are two H-assisted steps: NHOH+H→NH+H_2O and NHOH+H→NH_2OH. The former one is a concerted step, in which surface H transfers to O leading to the formation of H_2O; meanwhile, N−O bond is broken. The energy barrier and the reaction heat are 98.1 and −91.7 kJ·mol^{-1}, respectively. Unlike the N−O bond being broken in the H-assisted dissociation process, the N−O bond is slightly stretched from 1.408 to 1.444 Å in the process of hydrogenation NHOH to NH_2OH. The step is endothermic with a reaction energy of 30.1 kJ·mol^{-1}, and an activation energy barrier of 116.6 kJ·mol^{-1} is needed, as shown in Figure 5. It can be seen that steps 11 and 12 are favorable with little advantage from the kinetics.

3.2.4. Brief Summary about Active N and NH Formation. A feasible reaction path for the formation of active N and NH can be obtained from the above analysis, as shown in Path 1.

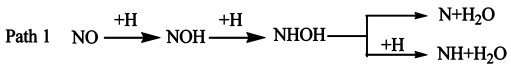

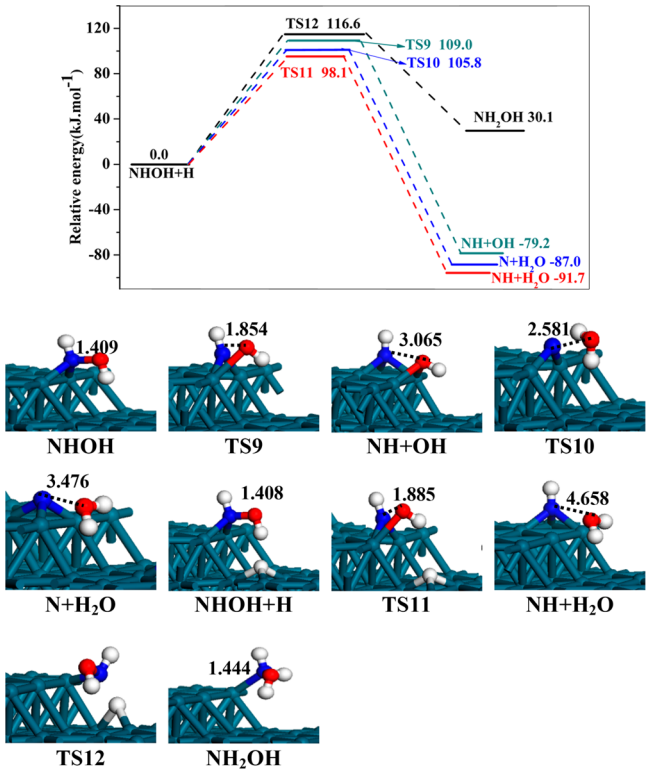

Figure 5. Potential energy diagram of correlated reactions of NHOH including ZPE correction together with corresponding configurations of initial states, transition states, and final states. Bond lengths are in angstroms.

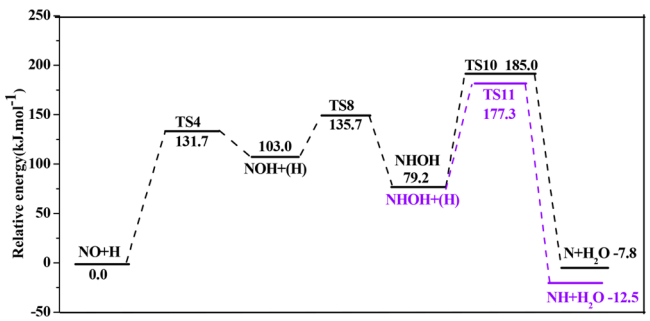

Figure 6. Potential energy diagram of the favorable routes for the formation of active N and NH including ZPE correction.

NO is liable to hydrogenate leading to the formation of NOH, as shown in Figure 6. And then, NHOH is generated as an important active intermediate via further hydrogenation of NOH. Furthermore, the N−O bond is broken leading to the formation of N or NH with a little energy barrier difference. The similar results were obtained by experiment methods, in which the dissociation of NO assisted by chemisorbed H atoms likely occurs on Pd/Al_2O_3.[76] However, it is different from that on the Pd(111) surface,[30] and the most favorable routes for the cleavage of N−O bond are NO+H→N+OH and NO+H→NH+O. N and NH intermediates are formed via different reaction steps, which are precursors for products N_2 and NH_3.

3.3. Formation of Products N_2, NH_3, and H_2O. *3.3.1. N_2 Formation from Active N.* Active N is the precursor of N_2. The formation of N_2 starting from active N intermediate and NO will be studied, and there are four different paths, as shown in Paths 2−5.

DOI: 10.1021/acs.jpcc.7b05024
J. Phys. Chem. C 2017, 121, 16399−16414

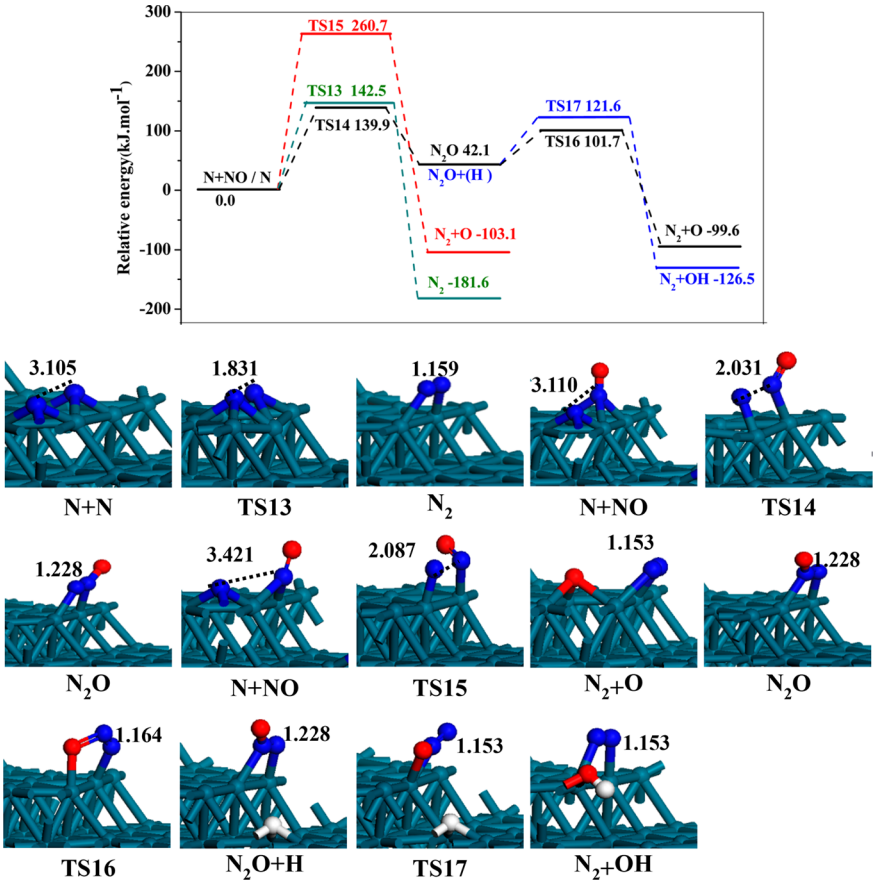

Figure 7. Potential energy diagram of the formation of N_2 via the active N path including ZPE correction together with corresponding configurations of initial states, transition states, and final states. Bond lengths are in angstroms.

Path 2 $N + N \rightarrow N_2$

Path 3 $N + NO \rightarrow N_2O \rightarrow N_2 + O$

Path 4 $N + NO \rightarrow N_2O \xrightarrow{+H} N_2 + OH$

Path 5 $N + NO \rightarrow N_2 + O$

Two adsorbed active N atoms directly combine with each other and generate N_2; the activation energy barrier is 142.5 kJ·mol^{-1}, and the reaction heat is −181.6 kJ·mol^{-1} (see Figure 7). When active N reacts with adsorbed NO, three possible paths are discussed. One is that N_2O is formed by overcoming an energy barrier of 139.9 kJ·mol^{-1}, which is with similar energy barrier to the direct combining path. Then, the dissociation of N_2O to N_2 and O is investigated with a little energy barrier of 59.6 kJ·mol^{-1} (Path 3). Certainly, N_2O may be dissociated with H assistance, leading to the formation of N_2 and OH (Path 4). However, a higher energy barrier of 79.5 kJ·mol^{-1} is needed for this step than that of direct N_2O dissociation. It is indicated that N_2O is an intermediate, leading to the formation of N_2; the same situation was investigated on the Rh(110) and Pd(110) surface.[77,78] In addition, N_2 emission via the decomposition of N_2O intermediate in a steady-state NO+CO+D_2 reaction on the stepped Pd(211) surface was investigated by Angle-resolved desorption,[79] whereas N_2O is a product desorbing from Pt(111), Rh(111), and Ni(111) surfaces without dissociation.[80−82] Comparing with the activation energies of N_2O dissociation with and without H assistance, the direct decomposition of N_2O is dominant for N_2 formation due to lower energy barrier, and the H-assisted path is less competitive. Path 5 is the adsorbed active N attacking the N of NO, leading to the formation of N_2 followed by N−O bond cleaving; meanwhile, O will be deposited on the surface. A large activation energy of 260.7 kJ·mol^{-1} is needed for the synergetic path. It can be seen that the favorable paths for the formation of N_2 via the active N path are N+N→N_2 and NO +N→N_2O→N_2+O.

3.3.2. N_2 Formation from N_2O_2 Dimer. N_2O_2 is an important adsorbed species on the metal surface in the process of NO reduction; both *cis*-N_2O_2 and *trans*-N_2O_2 are found on some metal surfaces.[25,64,66] When two NO molecules are adsorbed on two neighboring top sites on the Pd(211) surface though O, they spontaneously form the *cis*-N_2O_2 species without energy barrier. This trapezoid dimer is also found be a necessary intermediate for the formation of N_2O during NO reduction on the Au(111) surface.[25] We do not exhibit the formation process of *cis*-N_2O_2 in Figure 8 because it is a spontaneous elementary step and barrierless; an energy barrier of only 10.6 kJ·mol^{-1} is needed for this step on the Au(111) surface,[25] and an activation energy of −8.7 kJ·mol^{-1} is needed on the Pd(111) surface.[30] It is regretful that the formation of *trans*-N_2O_2 starting from two NO molecules has not been observed. However, it was investigated on the Au(111) and Pd(111) surfaces.[25,30] For the further reaction of *cis*-N_2O_2, the direct dissociation is first considered and studied. We try our best to find the transition state of this step but failed. A new reaction path for the N_2O_2 is provided where *cis*-N_2O_2 transforms into *trans*-N_2O_2 in the first step, and then the decomposition of *trans*-N_2O_2 occurs leading to the formation of N_2O. There are two energy barriers of 81.9 and 116.2 kJ·mol^{-1}

DOI: 10.1021/acs.jpcc.7b05024
J. Phys. Chem. C 2017, 121, 16399−16414

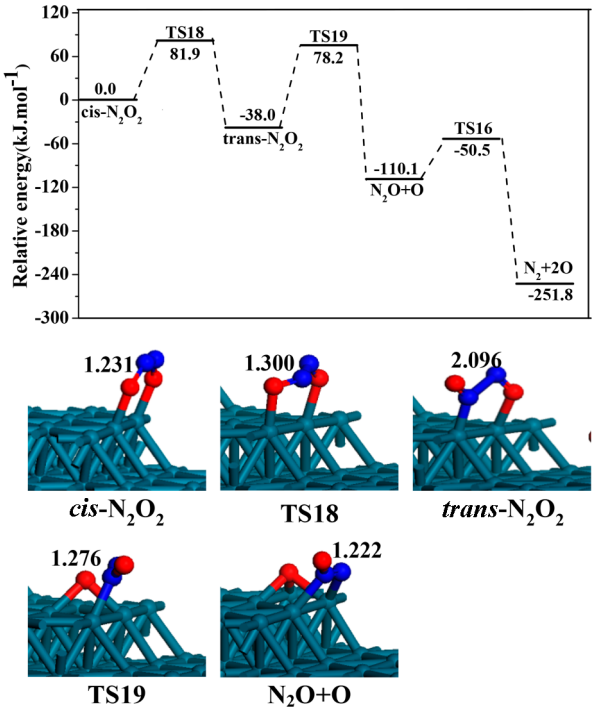

Figure 8. Potential energy diagram of the formation of N_2 via the dimer path including ZPE correction together with corresponding configurations of initial states, transition states, and final states. Bond lengths are in angstroms.

for these two steps. According to the above calculation results, we can conclude that the route of the *cis*-N_2O_2→*trans*-N_2O_2→N_2O +O is a possible path for the dissociation process of NO through $(NO)_2$ species. This result is different from that on Pd(111)[30] and Au(111) surfaces,[25] in which the most favorable path is that *cis*-N_2O_2 directly dissociates into N_2O and O. Then N_2O is directly decomposed into N_2 via the same step in Path 3 with a little energy barrier of 59.6 kJ·mol^{-1}, which is much lower than that of *trans*-N_2O_2 dissociation to generate N_2O (116.2 kJ·mol^{-1}). Additionally, the dissociation of *trans*-N_2O_2 is an exothermic process with 72.1 kJ·mol^{-1}. Both of them lead to the cleavage of N−O bond in N_2O easily to N_2 in this reaction system. Similarly, the activation barrier for N_2 production remained lower than that calculated for N_2O on Pt(111) and Pd(111) surfaces, also indicating that N_2 would be formed preferentially at the expense of N_2O.[29] In addition, the experiment shows that N_2O is an active and important intermediate for the formation of N_2,[79,32] and the production of N_2O and N_2 involved the same intermediates, *trans*-N_2O_2.[83] N_2O is also decomposed to N_2 on Rh(110) and Rh(100) surfaces.[84,85] The dimer path is feasible and N_2 emission from the decomposition of N_2O takes place below 500 K[32] on the Pd(211) surface.

$$\text{Path 6} \quad NO + NO \rightarrow \text{cis-}N_2O_2 \rightarrow \text{trans-}N_2O_2 \rightarrow N_2O + O \rightarrow N_2 + 2O$$

3.3.3. NH_3 Formation. The NH_3 formation involves two paths: the successive hydrogenation reactions of N atom and the successive hydrogenation of NH via the decomposition of NHOH. Certainly, the second path is included into the first one (see Path 7).

$$\text{Path 7} \quad N \xrightarrow{+H} NH \xrightarrow{+H} NH_2 \xrightarrow{+H} NH_3$$

It can be seen from Figure 9 that the hydrogenation reactions of NH_x ($x = 0-2$) (N+H→NH, NH+H→NH_2 and NH_2+H→NH_3)

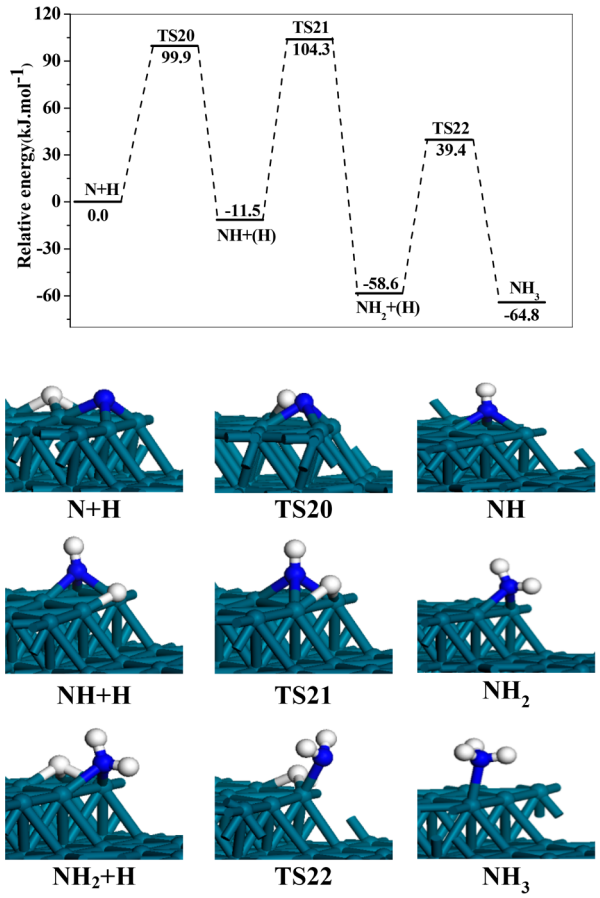

Figure 9. Potential energy diagram of the formation of NH_3 including ZPE correction together with corresponding configurations of initial states, transition states, and final states.

need to overcome energy barriers of 99.9, 115.8, and 98.0 kJ·mol^{-1}, respectively. Compared to energy barriers of forming NH_2 (87.8 kJ·mol^{-1}) and NH_3 (77.2 kJ·mol^{-1}) on the Pd(111) surface,[30] it is not conducive to the formation of NH_3 on the Pd(211) surface.

3.3.4. H_2O Formation. In the process of the reduction of NO by H_2, the O atom is mainly from the dissociation of N_2O and N_2O_2 as discussed above, OH is mainly from the decomposition of NHOH intermediate, and H_2O is the final presence form of O atom and OH. Two possible reactions are considered in this study for the formation of H_2O, as shown in Paths 8 and 9.

$$\text{Path 8} \quad O \xrightarrow{+H} OH \xrightarrow{+H} H_2O$$

$$\text{Path 9} \quad O \xrightarrow{+H} OH \xrightarrow{+OH} H_2O + O$$

The energy barrier for the hydrogenation of O atom is 123.0 kJ·mol^{-1}, which is an exothermic reaction with the energy of −54.3 kJ·mol^{-1}, as shown in Figure 10. Then both OH+H and OH+OH will lead to the formation of H_2O, and they need to overcome energy barriers of 91.7 and 135.5 kJ·mol^{-1}. It is obvious that the OH further hydrogenation reaction is more favorable.

3.4. General Discussion. *3.4.1. Main Paths for the Formation of N_2 and NH_3.* As discussed above, there are two possible pathways to the generation of N_2 on the Pd(211)

DOI: 10.1021/acs.jpcc.7b05024
J. Phys. Chem. C 2017, 121, 16399−16414

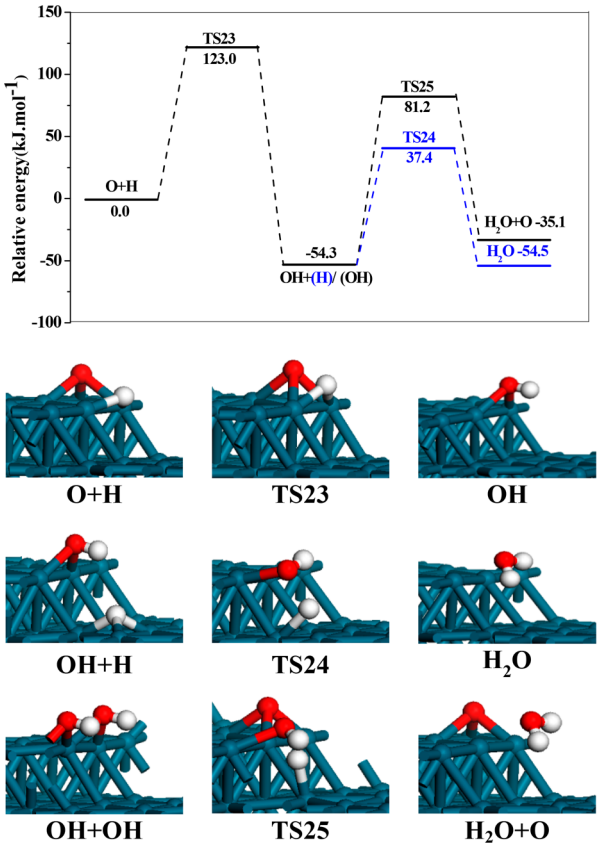

Figure 10. Potential energy diagram of the formation of H_2O including ZPE correction together with corresponding configurations of initial states, transition states, and final states.

surface. As shown in Figure 11, one of pathways is the active N path, and the active N is first formed via the favorable route: NO+H→NOH+H→NHOH→N, and then the following reaction (N+N→N_2 or NO+N→N_2O→N_2+O) will occurr. The highest energy barriers are 142.5 kJ·mol^{-1} for the combination of two active N, and 139.9 kJ·mol^{-1} for the formation of intermediate of N_2O. A similar activation method for NO is also investigated on the Pt(111) surface; the cleavage of N−O is via HNOH intermediate, and H addition weakens the multiple bonds in NO.[24] The other one is the dimer path, namely, 2NO→*cis*-N_2O_2→*trans*-N_2O_2→N_2O→N_2+O, in which the decomposition of *trans*-N_2O_2 into N_2O and O is the rate-determining step with an energy barrier of 116.2 kJ·mol^{-1}. N_2O_2 dimer can also exist on Ag(111) surface. Then the dissociation of N_2O into N_2 needs to overcome an energy barrier of 100.3 kJ·mol^{-1} on the Ag(111) surface.[64] The intermediate N_2O played an important role for N_2 emission during the reduction of NO on the Pd(211) surface.[79] The similar results show that N_2O is easily formed on Au(111) and Ag(111) surfaces with energy barriers of 32.8 and 26.0 kJ·mol^{-1},[25,64] respectively. It is worth noting that there are two different opinions for the formation of N_2O, NO dissociation, and the subsequent NO+N→N_2O mainly proceeding in other work.[79] However, a decomposition path of N_2O_2 (N_2O_2→N_2O+O) is the main source for N_2O by our study on the Pd(211) surface, which is consistent with the formation of N_2O via a bimolecular reaction between two adjacent chemisorbed NO molecules.[29] In any case, N_2O will be decomposed, leading to the emission of N_2. It can also be concluded that there are two competitive paths for N_2 emission during NO reduction on the Pd(211) surface, in which the highest activation energies of 142.5 and 139.9 kJ·mol^{-1} are for the active N path, and 116.2 kJ·mol^{-1} is for the dimer path. Comparing with the highest activation energy (152.4 kJ·mol^{-1}) occurring at the dissociation of NO bond for the formation of N_2 on the Pd(111) surface,[30] the barrier of the rate-determining step has declined for the N_2 emission, implying that the Pd(211) surface exhibits higher catalytic activity to the reduction of NO with H_2 than that on the Pd(111) surface.

For the formation of NH_3, the successive hydrogenation of N or NH is the feasible path, which are from the direct dissociation and H-assisted dissociation process of NHOH. No matter which path leads to NH_3, the rate-determining step is the hydrogenation of NO to NOH, and the energy barrier is 131.7 kJ·mol^{-1}.

3.4.2. Relative Selectivity of N_2 and NH_3. Microkinetic modeling was used to predict the relative product selectivity; meanwhile, surface coverage and reaction rates were also obtained.[86,87] All possible reaction steps for the formation of N_2 and NH_3 (as shown in Figure 11) are listed in Table 4, and the main formation steps for H_2O are also shown. Rate constants for all elementary steps are calculated based on the harmonic transition state theory (TST)[88] in eq 4:

$$k = \nu_i \exp\left(\frac{-E_a}{RT}\right) \tag{4}$$

where ν_i is the pre-exponential factor, E_a is the ZPE-corrected energy barrier, and T is the temperature. The pre-exponential factor ν_i of each reaction pathway was calculated by eq 5:[89]

$$\nu_i = \frac{k_B T}{h} \frac{\prod_{i=1}^{3N}\left[1 - \exp\left(-\frac{hf_i^{IS}}{k_B T}\right)\right]}{\prod_{i=1}^{3N-1}\left[1 - \exp\left(-\frac{hf_i^{TS}}{k_B T}\right)\right]} \tag{5}$$

where f_i^{IS} are the vibrational frequencies at the initial state, and f_i^{TS} are the vibrational frequencies at the transition state (excluding the imaginary one).

The related reactions and the rate constants at the temperature range of 300−700 K are shown in Table 5. The site balance of the intermediate species involved in the reaction and free site (*) can be written as follows:

$$\theta_H + \theta_{NO} + \theta_{trans\text{-}N_2O_2} + \theta_{cis\text{-}N_2O_2} + \theta_{NOH} + \theta_{NHOH} + \theta_N + \theta_{NH} + \theta_{NH_2} + \theta_O + \theta_{OH} + \theta_{N_2O} + \theta^* = 1 \tag{6}$$

The coverages of surface NO, H, and *cis*-N_2O_2 are obtained by eqs 7−9:

$$\theta_{NO} = P_{NO} K_{NO} \theta^* \tag{7}$$

$$\theta_H = \sqrt{P_{H_2} K_{H_2}}\, \theta^* \tag{8}$$

$$\theta_{cis\text{-}N_2O_2} = P_{NO}{}^2 K_{cis\text{-}N_2O_2} \theta^* \tag{9}$$

The adsorption processes of the NO, H_2, and *cis*-N_2O_2 were also assumed to be in equilibrium, and the equilibrium constant K_{eq} was estimated according to eq 10:

$$K_{eq} = \exp[-(\Delta E_{ads} - T\Delta S)/RT] \tag{10}$$

where ΔE_{ads} is the adsorption energy of NO, H_2, and *cis*-N_2O_2, respectively.

DOI: 10.1021/acs.jpcc.7b05024
J. Phys. Chem. C 2017, 121, 16399−16414

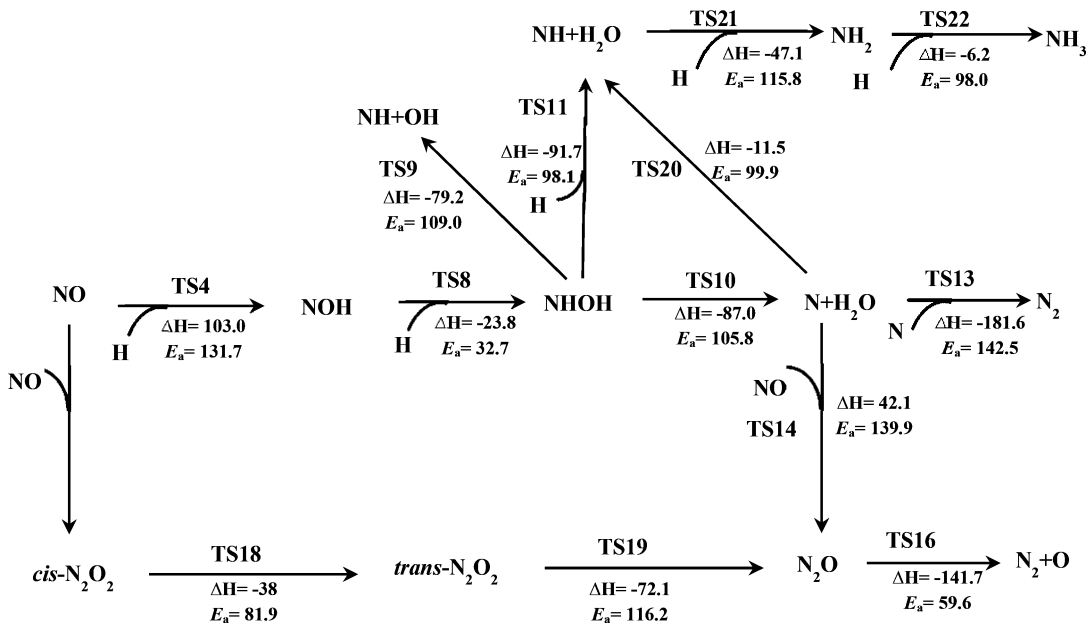

Figure 11. Possible formation pathway of N_2 and NH_3 during the reaction of NO by H_2 on the stepped Pd(211) surface with the reaction energies and activation barriers of elementary reactions. The unit is kJ·mol^{-1}.

Table 4. Related Reactions and the Representation of the Corresponding Rate Constant

reaction	rate constant	reaction	rate constant
NO* + H* → NOH* + *	k_4	N* + H* → NH* + *	k_{12}
NOH* + H* → NHOH* + *	k_5	NH* + H* → NH_2* + *	k_{13}
NHOH* + * → NH* + OH*	k_6	NH_2* + H* → NH_3* + *	k_{14}
NHOH* + * → N* + H_2O + *	k_7	*cis*-N_2O_2* + * → *trans*-N_2O_2* + *	k_{15}
NHOH* + H* → NH* + H_2O + *	k_8	*trans*-N_2O_2* + * → N_2O* + O*	k_{16}
N* + N* → N_2 + 2*	k_9	O* + H* → OH* + *	k_{17}
N* + NO* → N_2O* + *	k_{10}	OH* + H* → H_2O + 2*	k_{18}
N_2O* + * → N_2 + O* + *	k_{11}		

ΔS is the entropy change of NO, H_2 and *cis*-N_2O_2 induced by adsorption, respectively. It can be obtained by the eq 11:

$$\Delta S = S_{\text{adsorbate}} - S_{\text{gas}} \tag{11}$$

$$S_{\text{adsorbate}} = \sum_{i=1}^{3N}\left[-R\ln\left(1-\exp\left(-\frac{hf_i}{k_BT}\right)\right) + \frac{N_A hf_i}{T}\frac{\exp\left(-\frac{hf_i}{k_BT}\right)}{1-\exp\left(-\frac{hf_i}{k_BT}\right)}\right] \tag{12}$$

where $S_{\text{adsorbate}}$ is the entropy of NO, H_2, and *cis*-N_2O_2 adsorbing on the Pd(211) surface, which can be obtained according to the eq 12, and f_i are the vibrational frequencies of adsorbates. S_{gas} is the gas phase entropy. The gas phase entropies of NO and H_2 were obtained from the NIST Chemistry WebBook.[90] For *cis*-N_2O_2, the gas phase entropy was represented by that of two NO molecules, since two NO molecules adsorbing on two neighboring top sites can spontaneously form the *cis*-N_2O_2 species on the Pd(211) surface.

In this study, microkinetic modeling pressures were at P_{NO} = 100 Pa and P_{H2}= 500 Pa.[30] The coverage of other surface species can be described according to the steady-state approximation, where the rates for the production and the consumption of each species were assumed to be equals:

$$\theta_{trans\text{-}N_2O_2}:\quad \frac{d\theta_{trans\text{-}N_2O_2}}{dt} = k_{15}\theta_{cis\text{-}N_2O_2}\theta^* - k_{16}\theta_{trans\text{-}N_2O_2}\theta^* = 0 \tag{13}$$

$$\theta_{\text{NOH}}:\quad \frac{d\theta_{\text{NOH}}}{dt} = k_4\theta_{\text{NO}}\theta_{\text{H}} - k_5\theta_{\text{NOH}}\theta_{\text{H}} = 0 \tag{14}$$

$$\theta_{\text{NHOH}}:\quad \frac{d\theta_{\text{NHOH}}}{dt} = k_5\theta_{\text{NOH}}\theta_{\text{H}} - k_6\theta_{\text{NHOH}}\theta^* - k_7\theta_{\text{NHOH}}\theta^* - k_8\theta_{\text{NHOH}}\theta_{\text{H}} = 0 \tag{15}$$

$$\theta_{\text{N}}:\quad \frac{d\theta_{\text{N}}}{dt} = k_7\theta_{\text{NHOH}}\theta^* - k_9\theta_{\text{N}}^2 - k_{10}\theta_{\text{N}}\theta_{\text{NO}} - k_{12}\theta_{\text{N}}\theta_{\text{H}} = 0 \tag{16}$$

$$\theta_{\text{NH}}:\quad \frac{d\theta_{\text{NH}}}{dt} = k_6\theta_{\text{NHOH}}\theta^* + k_8\theta_{\text{NHOH}}\theta_{\text{H}} + k_{12}\theta_{\text{N}}\theta_{\text{H}} - k_{13}\theta_{\text{NH}}\theta_{\text{H}} = 0 \tag{17}$$

DOI: 10.1021/acs.jpcc.7b05024
J. Phys. Chem. C 2017, 121, 16399−16414

Table 5. Reaction Equilibrium Constants and Rate Constants in the Different Reaction Paths (300 K ≤ T ≤ 700 K)

	rate constants/equilibrium constants								
	300 K	350 K	400 K	450 K	500 K	550 K	600 K	650 K	700 K
K_1	2.419×10^{28}	1.195×10^{23}	1.298×10^{19}	1.103×10^{16}	3.941×10^{13}	3.995×10^{11}	8.838×10^{9}	3.558×10^{8}	2.291×10^{7}
K_2	3.009×10^{3}	2.183×10^{1}	5.925×10^{-1}	3.819×10^{-2}	4.468×10^{-3}	8.011×10^{-4}	1.969×10^{-4}	6.150×10^{-5}	2.312×10^{-5}
K_3	5.470×10^{8}	3.011×10^{6}	6.289×10^{4}	3.212×10^{3}	3.069×10^{2}	4.624×10^{1}	9.784	2.684	9.017×10^{-1}
k_4	5.061×10^{-11}	1.071×10^{-7}	3.379×10^{-5}	2.993×10^{-3}	1.087×10^{-1}	2.065	2.408×10	1.929×10^{2}	1.150×10^{3}
k_5	4.570×10^{6}	3.231×10^{7}	1.409×10^{8}	4.445×10^{8}	1.117×10^{9}	2.375×10^{9}	4.459×10^{9}	7.603×10^{9}	1.202×10^{10}
k_6	1.025×10^{-6}	6.215×10^{-4}	7.737×10^{-2}	3.344	6.878×10	8.232×10^{2}	6.557×10^{3}	3.813×10^{4}	1.731×10^{5}
k_7	2.321×10^{-6}	1.146×10^{-3}	1.224×10^{-1}	4.701	8.800×10	9.755×10^{2}	7.290×10^{3}	4.019×10^{4}	1.743×10^{5}
k_8	1.190×10^{-4}	3.939×10^{-2}	3.121	9.510×10	1.480×10^{3}	1.412×10^{4}	9.311×10^{4}	4.618×10^{5}	1.830×10^{6}
k_9	1.315×10^{-12}	5.466×10^{-9}	2.859×10^{-6}	3.747×10^{-4}	1.860×10^{-2}	4.552×10^{-1}	6.552	6.267×10	4.346×10^{2}
k_{10}	5.426×10^{-12}	1.941×10^{-8}	9.049×10^{-6}	1.083×10^{-3}	4.993×10^{-2}	1.150	1.573×10	1.441×10^{2}	9.622×10^{2}
k_{11}	3.112×10^{2}	1.105×10^{4}	1.633×10^{5}	1.340×10^{6}	7.271×10^{6}	2.916×10^{7}	9.312×10^{7}	2.494×10^{8}	5.814×10^{8}
k_{12}	3.308×10^{-5}	1.246×10^{-2}	1.088	3.567×10	5.880×10^{2}	5.864×10^{3}	4.006×10^{4}	2.044×10^{5}	8.290×10^{5}
k_{13}	3.907×10^{-8}	3.495×10^{-5}	5.834×10^{-3}	3.170×10^{-1}	7.830	1.088×10^{2}	9.817×10^{2}	6.343×10^{3}	3.150×10^{4}
k_{14}	1.081×10^{-4}	3.534×10^{-2}	2.741	8.129×10	1.228×10^{3}	1.136×10^{4}	7.262×10^{4}	3.495×10^{5}	1.345×10^{6}
k_{15}	1.497×10^{-2}	1.781	6.443×10	1.052×10^{3}	9.849×10^{3}	6.144×10^{4}	2.827×10^{5}	1.029×10^{6}	3.115×10^{6}
k_{16}	5.210×10^{-9}	3.908×10^{-6}	5.598×10^{-4}	2.664×10^{-2}	5.869×10^{-1}	7.385	6.106×10	3.656×10^{2}	1.698×10^{3}
k_{17}	3.275×10^{-9}	4.480×10^{-6}	1.023×10^{-3}	7.062×10^{-2}	2.106	3.408×10	3.483×10^{2}	2.497×10^{3}	1.355×10^{4}
k_{18}	2.218×10^{-3}	5.670×10^{-1}	3.724×10	9.829×10^{2}	1.365×10^{4}	1.185×10^{5}	7.225×10^{5}	3.351×10^{6}	1.253×10^{7}

$$\theta_{NH_2}: \quad \frac{d\theta_{NH_2}}{dt} = k_{13}\theta_{NH}\theta_H - k_{14}\theta_{NH_2}\theta_H = 0 \tag{18}$$

$$\theta_O: \quad \frac{d\theta_O}{dt} = k_{16}\theta_{trans\text{-}N_2O_2}\theta^* + k_{11}\theta_{N_2O}\theta^* - k_{17}\theta_O\theta_H = 0 \tag{19}$$

$$\theta_{OH}: \quad \frac{d\theta_{OH}}{dt} = k_{17}\theta_O\theta_H + k_6\theta_{NHOH}\theta^* - k_{18}\theta_{OH}\theta_H = 0 \tag{20}$$

$$\theta_{N_2O}: \quad \frac{d\theta_{N_2O}}{dt} = k_{16}\theta_{trans\text{-}N_2O_2}\theta^* + k_{10}\theta_N\theta_{NO} - k_{11}\theta_{N_2O}\theta^* = 0 \tag{21}$$

From eqs 6−21, the coverage of all reactive species can be obtained, as shown in Table 6.

The formation paths for N_2 and NH_3 are also obtained from the analysis of rate constants. Both the active N path and the dimer path contribute to the formation of N_2, and the favorable approach of producing NH_3 is that the stepwise hydrogenation of active N or NH leads to the formation of NH_3. Comparing with the rate constant of each elementary step in these paths, N+N → N_2 and NO+N → N_2O are the rate-limiting steps for the formation of N_2 via the active N path, and *trans*-N_2O_2 → N_2O+O is the rate-limiting step via the dimer path. The rate-limiting step for NH_3 formation is NO+H → NOH. This is in agreement with the result of analysis by activation energy barrier.

The formation rate of one product is proportional to the concentration of reactants and the reaction rate constant.[91] In addition, different rate-limiting steps control the relative distribution of products in the formation of N_2 and NH_3, respectively. Therefore, the formation rates of N_2 and NH_3 are expressed as eqs 22−24:

$$r_{N_2\text{activeN}} = \frac{1}{2}k_9\theta_{NO}\theta_H + \frac{1}{2}k_{10}\theta_{NO}\theta_H \tag{22}$$

$$r_{N_2\text{dimer}} = k_{16}\theta_{cis\text{-}N_2O_2} \tag{23}$$

$$r_{NH_3} = k_4\theta_{NO}\theta_H \tag{24}$$

Therefore, the relative selectivity of N_2 and NH_3 can be obtained by eqs 25−28:

$$s_{N_2\text{activeN}} = \frac{r_{N_2\text{activeN}}}{r_{NH_3} + r_{N_2\text{activeN}} + r_{N_2\text{dimer}}} \tag{25}$$

$$s_{N_2\text{dimer}} = \frac{r_{N_2\text{dimer}}}{r_{NH_3} + r_{N_2\text{activeN}} + r_{N_2\text{dimer}}} \tag{26}$$

$$s_{NH_3} = \frac{r_{NH_3}}{r_{NH_3} + r_{N_2\text{activeN}} + r_{N_2\text{dimer}}} \tag{27}$$

$$s_{N_2} = s_{N_2\text{activeN}} + s_{N_2\text{dimer}} \tag{28}$$

The relative selectivity of N_2 and NH_3 at the temperature range of 300−700 K is shown in Figure 12. The selectivity of N_2 is higher than that of NH_3 under the low temperature; however, it decreases with the increasing of temperature. NH_3 is the main product when the temperature is above about 500 K. This is in agreement with the dissociation of N_2O to N_2 predominantly formed during the cold start engine, and surface N and H coverage increase with the temperature increasing, which favors the production of NH_3 on Rh/Al_2O_3.[83] Similar results are also obtained on the Rh/SiO_2 catalyst, in which N_2O is easily formed under low temperature and NH_3 is the main product at high temperature.[92]

Moreover, the formation of N_2 is mainly via the dimer path below about 525 K. With increasing temperature, N_2 formation via the dimer path decreases quickly, whereas the formation of N_2 via the active N path increases, indicating that high temperature is advantageous to the formation of active N. It can be seen that the dissociation of N_2O_2 to N_2O, and then N_2 formation followed by the decomposition of N_2O prevails below about 525 K, which is in agreement with the experiment that N_2 emission is from the intermediate N_2O decomposition below ∼500 K on the stepped Pd(211) surface,[79] and the N_2O decomposition channel is prevalent at low temperature.[32] It is also obtained that the concentration of the active N increases with the temperature increasing, and the active N is the important intermediate for the N_2 generation under high temperature,

DOI: 10.1021/acs.jpcc.7b05024
J. Phys. Chem. C 2017, 121, 16399−16414

Table 6. Surface Coverage of Different Species at Different Temperatures (300 K ≤ T ≤ 700 K)

	300 K	350 K	400 K	450 K	500 K	550 K	600 K	650 K	700 K
θ^*	4.128×10^{-31}	8.344×10^{-26}	7.658×10^{-22}	8.981×10^{-19}	2.502×10^{-16}	2.455×10^{-14}	1.104×10^{-12}	2.724×10^{-11}	4.204×10^{-10}
θ_{NO}	9.987×10^{-1}	9.969×10^{-1}	9.942×10^{-1}	9.906×10^{-1}	9.861×10^{-1}	9.810×10^{-1}	9.755×10^{-1}	9.695×10^{-1}	9.632×10^{-1}
θ_H	2.159×10^{-25}	3.237×10^{-21}	4.294×10^{-18}	1.138×10^{-15}	9.802×10^{-14}	3.734×10^{-12}	7.720×10^{-11}	9.981×10^{-10}	8.926×10^{-9}
$\theta_{cis\text{-}N2O2}$	1.242×10^{-23}	1.822×10^{-20}	4.537×10^{-18}	3.430×10^{-16}	1.118×10^{-14}	1.967×10^{-13}	2.173×10^{-12}	1.675×10^{-11}	9.720×10^{-11}
$\theta_{trans\text{-}N2O2}$	3.568×10^{-17}	8.303×10^{-15}	5.222×10^{-13}	1.355×10^{-11}	1.876×10^{-10}	1.636×10^{-9}	1.006×10^{-8}	4.716×10^{-8}	1.784×10^{-7}
θ_{NOH}	1.106×10^{-17}	3.304×10^{-15}	2.384×10^{-13}	6.669×10^{-12}	9.603×10^{-11}	8.528×10^{-10}	5.267×10^{-9}	2.460×10^{-8}	9.216×10^{-8}
θ_{NHOH}	4.249×10^{-7}	2.710×10^{-6}	1.076×10^{-5}	3.117×10^{-5}	7.241×10^{-5}	1.433×10^{-4}	2.517×10^{-4}	4.030×10^{-4}	6.000×10^{-4}
θ_N	0.000	0.000	0.000	0.000	0.000	3.161×10^{-15}	1.319×10^{-13}	3.160×10^{-12}	4.743×10^{-11}
θ_{NH}	1.294×10^{-3}	3.054×10^{-3}	5.758×10^{-3}	9.352×10^{-3}	1.369×10^{-2}	1.860×10^{-2}	2.390×10^{-2}	2.941×10^{-2}	3.501×10^{-2}
θ_{NH2}	4.675×10^{-7}	3.020×10^{-6}	1.226×10^{-5}	3.646×10^{-5}	8.727×10^{-5}	1.782×10^{-4}	3.230×10^{-4}	5.338×10^{-4}	8.199×10^{-4}
θ_{N2O}	5.973×10^{-28}	2.935×10^{-24}	1.790×10^{-21}	2.694×10^{-19}	1.514×10^{-17}	4.981×10^{-9}	1.970×10^{-8}	6.495×10^{-8}	1.799×10^{-7}
θ_O	2.171×10^{-22}	3.733×10^{-19}	1.019×10^{-16}	8.067×10^{-15}	2.668×10^{-13}	2.803×10^{-5}	7.530×10^{-5}	1.771×10^{-4}	3.636×10^{-4}
θ_{OH}	3.756×10^{-16}	7.656×10^{-14}	3.987×10^{-12}	8.368×10^{-11}	9.315×10^{-10}	1.461×10^{-8}	6.896×10^{-8}	2.571×10^{-7}	7.837×10^{-7}

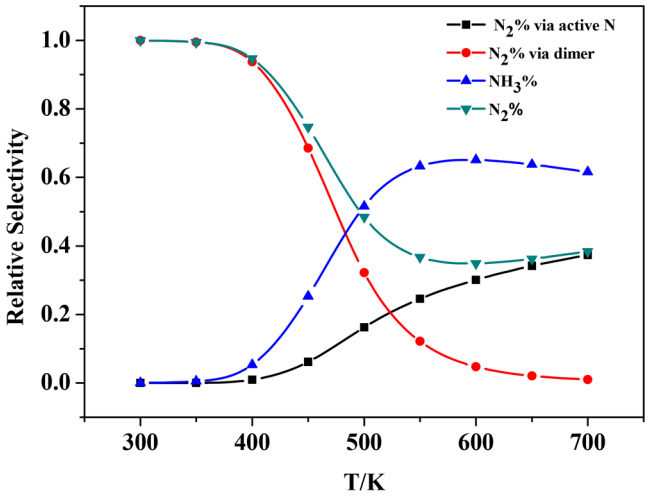

Figure 12. Relative selectivity for the formation of N_2 and NH_3 on different temperatures (300 ≤ T ≤ 700 K).

which is in agreement with the experiment where the formation of N_2 is via the path of N+N → N_2 above ~500 K.[79]

4. CONCLUSIONS

In this work, the reduction of NO by H_2 on the stepped Pd(211) surface has been studied by using the periodic density functional theory method. NO tends to hydrogenate, leading to the formation of NOH, rather than direct dissociation. Then NHOH is generated through the hydrogenation of NOH. N and NH are formed followed by the N−O bond cleavage of NHOH on the Pd(211) surface.

In addition, N_2 emission paths are studied, including the active N path and the dimer path. The result shows that the dimer path is the main route for the formation of N_2 at low temperature, but the active N path is changed into the main path for N_2 generation at high temperature. It is different from that on the Pd(111) surface, and the energy barrier for the rate-determining step shows that the formation of N_2 on the stepped Pd(211) surface is easier than that on the flat Pd(111) surface. Additionally, the selectivity of N_2 is higher than that of NH_3 on the stepped Pd(211) surface below about 500 K.

■ AUTHOR INFORMATION

Corresponding Author

*Address: No. 79 West Yingze Street, Taiyuan 030024, China. Tel.: +86 351 6018239; Fax: +86 351 6041237; E-mail address: wangbaojun@tyut.edu.cn.

ORCID

Baojun Wang: 0000-0002-9069-6720

Notes

The authors declare no competing financial interest.

■ ACKNOWLEDGMENTS

We gratefully acknowledge financial support from the National Natural Science Foundation of China (Grant Nos. 21576178 and 21476155), Research Project Supported by Shanxi Scholarship Council of China (No. 2016-030) and the Program for the Innovative Talents of Higher Learning Institutions of Shanxi.

■ REFERENCES

(1) Su, Y. X.; Zhao, B. T.; Deng, W. Y. NO Reduction by Methane over Iron Oxides: Characteristics and Mechanisms. *Fuel* **2015**, *160*, 80−86.

DOI: 10.1021/acs.jpcc.7b05024
J. Phys. Chem. C 2017, 121, 16399−16414

(2) Patel, A.; Shukla, P.; Chen, J. L.; Rufford, T. E.; Wang, S. B.; Rudolph, V.; Zhu, Z. H. Structural Sensitivity of Mesoporous Alumina for Copper Catalyst Loading Used for NO Reduction in Presence of CO. *Chem. Eng. Res. Des.* **2015**, *101*, 27−43.
(3) Zhang, X. L.; Lu, Z. S.; Tang, Y. N.; Fu, Z. M.; Ma, D. W.; Yang, Z. X. A Density Function Theory Study on the NO Reduction on Nitrogen Doped Graphene. *Phys. Chem. Chem. Phys.* **2014**, *16*, 20561−20569.
(4) Calatayud, M.; Mguig, B.; Minot, C. Modeling Catalytic Reduction of NO by Ammonia over V_2O_5. *Surf. Sci. Rep.* **2004**, *55*, 169−236.
(5) Gao, X.; Du, X. S.; Jiang, Y.; Zhang, Y.; Luo, Z. Y.; Cen, K. F. A DFT Study on the Behavior of NO_2 in the Selective Catalytic Reduction of Nitric Oxides with Ammonia on a V_2O_5 Catalyst Surface. *J. Mol. Catal. A: Chem.* **2010**, *317*, 46−53.
(6) Sun, C. Z.; Dong, L. H.; Yu, W. J.; Liu, L. C.; Li, H.; Gao, F.; Dong, L.; Chen, Y. Promotion Effect of Tungsten Oxide on SCR of NO with NH_3 for the V_2O_5−WO_3/$Ti_{0.5}Sn_{0.5}O_2$ Catalyst: Experiments Combined with DFT Calculations. *J. Mol. Catal. A: Chem.* **2011**, *346*, 29−38.
(7) Peng, Y.; Li, J. H.; Chen, L.; Chen, J.; Han, J.; Zhang, H.; Han, W. Alkali Metal Poisoning of a CeO_2-WO_3 Catalyst Used in the Selective Catalytic Reduction of NO_x with NH_3: An Experimental and Theoretical Study. *Environ. Sci. Technol.* **2012**, *46*, 2864−2869.
(8) Peng, Y.; Liu, Z. M.; Niu, X. W.; Zhou, L.; Fu, C. W.; Zhang, H.; Li, J. H.; Han, W. Manganese Doped CeO_2−WO_3 Catalysts for the Selective Catalytic Reduction of NO_x with NH_3: An Experimental and Theoretical Study. *Catal. Commun.* **2012**, *19*, 127−131.
(9) Yao, H. C.; Chen, Y.; Zhao, Z.; Wei, Y. C.; Liu, Z. C.; Zhai, D.; Liu, B. J.; Xu, C. M. Periodic DFT Study on Mechanism of Selective Catalytic Reduction of NO via NH_3 and O_2 over the V_2O_5(001) Surface: Competitive Sites and Pathways. *J. Catal.* **2013**, *305*, 67−75.
(10) Wang, L. F.; Yin, C. Y.; Yang, R. T. Selective Catalytic Reduction of Nitric Oxide with Hydrogen on Supported Pd: Enhancement by Hydrogen Spillover. *Appl. Catal., A* **2016**, *514*, 35−42.
(11) Wang, L. F.; Chen, H.; Yuan, M. H.; Rivillon, S.; Klingenberg, E. H.; Li, J. X.; Yang, R. T. Selective Catalytic Reduction of Nitric Oxide by Hydrogen over Zn-ZSM-5 and Pd and Pd/Ru Based Catalysts. *Appl. Catal., B* **2014**, *152*−*153*, 162−171.
(12) Okumura, K.; Motohiro, T.; Sakamoto, Y.; Shinjoh, H. Effect of Combination of Noble Metals and Metal Oxide Supports on Catalytic Reduction of NO by H_2. *Surf. Sci.* **2009**, *603*, 2544−2550.
(13) de Wolf, C. A.; Nieuwenhuys, B. E. The NO-H_2 Reaction over Pd(111). *Surf. Sci.* **2000**, *469*, 196−203.
(14) Da Costa, P.; Modén, B.; Meitzner, G. D.; Lee, D. K.; Iglesia, E. Spectroscopic and Chemical Characterization of Action and Inactive Cu Species in NO Decomposition Catalysts Based on Cu-ZSM5. *Phys. Chem. Chem. Phys.* **2002**, *4*, 4590−4601.
(15) Modén, B.; Da Costa, P.; Fonfé, B.; Lee, D. K.; Iglesia, E. Kinetics and Mechanism of Steady-State Catalytic NO Decomposition Reactions on Cu-ZSM-5. *J. Catal.* **2002**, *209*, 75−86.
(16) Lobree, L. J.; Aylor, A. W.; Reimer, J. A.; Bell, A. T. NO Reduction by CH_4 in the Presence of O_2 over Pd-H-ZSM-5. *J. Catal.* **1999**, *181*, 189−204.
(17) Lobree, L. J.; Hwang, I. C.; Reimer, J. A.; Bell, A. T. An In Situ Infrared Study of NO Reduction by C_3H_8 over Fe-ZSM-5. *Catal. Lett.* **1999**, *63*, 233−240.
(18) Granger, P.; Dathy, C.; Lecomte, J. J.; Leclercq, L.; Prigent, M.; Mabilon, G.; Leclercq, G. Kinetics of the NO and CO Reaction over Platinum Catalysts. *J. Catal.* **1998**, *173*, 304−314.
(19) Hecker, W. C.; Bell, A. T. Reduction of NO by CO over Silica-Supported Rhodium: Infrared and Kinetic Studies. *J. Catal.* **1983**, *84*, 200−215.
(20) Hecker, W. C.; Bell, A. T. Reduction of NO by H_2-CO Mixtures over Silica-Supported Rhodium: Infrared and Kinetic Studies. *J. Catal.* **1984**, *88*, 289−299.
(21) Shustorovich, E.; Bell, A. T. Decomposition and Reduction of NO on Transition Metal Surfaces: Bond Order Conservation Morse Potential Analysis. *Surf. Sci.* **1993**, *289*, 127−138.
(22) Huai, L. Y.; Wang, H.; He, C. Z.; Wen, H.; Yi, W. C.; Liu, J. Y. Effect of Subsurface Oxygen on Selective Catalytic Reduction of NO by H_2 on Pt(100): A First-Principles Study. *J. Phys. Chem. C* **2015**, *119*, 24819−24826.
(23) Farberow, C. A.; Dumesic, J. A.; Mavrikakis, M. Density Functional Theory Calculations and Analysis of Reaction Pathways for Reduction of Nitric Oxide by Hydrogen on Pt(111). *ACS Catal.* **2014**, *4*, 3307−3319.
(24) Hibbitts, D. D.; Jiménez, R.; Yoshimura, M.; Weiss, B.; Iglesia, E. Catalytic NO Activation and NO−H_2 Reaction Pathways. *J. Catal.* **2014**, *319*, 95−109.
(25) Wang, Y. Y.; Zhang, D. J.; Yu, Z. Y.; Liu, C. B. Mechanism of N_2O Formation During NO Reduction on the Au(111) Surface. *J. Phys. Chem. C* **2010**, *114*, 2711−2716.
(26) Huai, L. Y.; Su, T.; Wen, H.; Jin, X.; Liu, J. Y. NO Reduction by H_2 on the Rh(111) and Rh(221) Surfaces: A Mechanistic and Kinetic Study. *J. Phys. Chem. C* **2016**, *120*, 5410−5419.
(27) Renème, Y.; Dhainaut, F.; Granger, P. Kinetics of the NO/H_2/O_2 Reactions on Natural Gas Vehicle Catalysts—Influence of Rh Addition to Pd. *Appl. Catal., B* **2012**, *111*, 424−432.
(28) Zhang, Q. Q.; Lv, L. F.; Zhu, J. X.; Wang, X. Q.; Wang, J.; Shen, M. Q. The Effect of CO on NO Reduction over Pt/Pd-Based NSR Catalysts at Low Temperature. *Catal. Sci. Technol.* **2013**, *3*, 1069−1077.
(29) Dhainaut, F.; Pietrzyk, S.; Granger, P. Kinetics of the NO/H_2 Reaction on Pt/$LaCoO_3$: A Combined Theoretical and Experimental Study. *J. Catal.* **2008**, *258*, 296−305.
(30) Huai, L. Y.; He, C. Z.; Wang, H.; Wen, H.; Yi, W. C.; Liu, J. Y. NO Dissociation and Reduction by H_2 on Pd(111): A First-Principles Study. *J. Catal.* **2015**, *322*, 73−83.
(31) Nakamura, I.; Fujitani, T.; Hamada, H. Adsorption and Decomposition of NO on Pd Surfaces. *Surf. Sci.* **2002**, *514*, 409−413.
(32) Matsushima, T.; Kokalj, A.; Orita, H.; Kubo, T.; Sakurai, M.; Kondo, T.; Nakamura, J. N_2 Emission-Channel Change in NO Reduction over Stepped Pd(211) by Angle-Resolved Desorption. *Surf. Sci.* **2012**, *606*, 1029−1036.
(33) Beck, D. E.; Heitzinger, J. M.; Avoyan, A.; Koel, B. E. Tuning the Chemistry of Metal Surfaces: I. Adsorption and Reaction of NO and N_2O on Ultrathin Pd Films on Ta(110). *Surf. Sci.* **2001**, *491*, 48−62.
(34) Ikai, M.; Tanaka, K. Spatial Distribution of N_2, N_2O, and NO Desorbing from a Pd(211) Surface. *J. Chem. Phys.* **1999**, *110*, 7031−7036.
(35) Ramsier, R. D.; Gao, Q.; Waltenburg, H. N.; Yates, J. T., Jr Thermal Dissociation of NO on Pd Surfaces: The Influence of Step Sites. *J. Chem. Phys.* **1994**, *100*, 6837−6845.
(36) Ramsier, R. D.; Gao, Q.; Waltenburg, H. N.; Lee, K. W.; Nooij, O. W.; Lefferts, L.; Yates, J. T., Jr NO Adsorption and Thermal Behavior on Pd Surfaces: A Detailed Comparative Study. *Surf. Sci.* **1994**, *320*, 209−237.
(37) Hammer, B. Reactivity of a Stepped Surface NO Dissociation on Pd(211). *Faraday Discuss.* **1998**, *110*, 323−333.
(38) Ren, Y.; Zhang, S.; Li, H. Electro-Oxidation of Methanol on SnO_2-Promoted Pd/MWCNTs Catalysts in Alkaline Solution. *Int. J. Hydrogen Energy* **2014**, *39*, 288−296.
(39) Ren, Y. B.; Zhang, S. C.; Lin, R. X.; Wei, X. Electro-Catalytic Performance of Pd Decorated Cu Nanowires Catalyst for the Methanol Oxidation. *Int. J. Hydrogen Energy* **2015**, *40*, 2621−2630.
(40) Orita, H.; Itoh, N.; Inada, Y. A Comparison of CO Adsorption on Pt(211), Ni(211), and Pd(211) Surface Using Density Functional Theory. *Surf. Sci.* **2004**, *571* (1−3), 161−172.
(41) Lahti, M.; Nivalainen, N.; Puisto, A.; Alatalo, M. O_2 Dissociation on Pd(211) and Cu(211) Surfaces. *Surf. Sci.* **2007**, *601* (18), 3774−3777.
(42) Lin, S.; Ma, J. Y.; Zhou, L. S.; Huang, C. J.; Xie, D. Q.; Guo, H. Influence of Step Defects on Methanol Decomposition: Periodic Density Functional Studies on Pd(211) and Kinetic Monte Carlo Simulations. *J. Phys. Chem. C* **2013**, *117* (1), 451−459.
(43) Yang, B.; Burch, R.; Hardacre, C.; Hu, P.; Hughes, P. Mechanistic Study of 1,3-Butadiene Formation in Acetylene Hydrogenation over the Pd-Based Catalysts Using Density Functional Calculations. *J. Phys. Chem. C* **2014**, *118*, 1560−1567.

DOI: 10.1021/acs.jpcc.7b05024
J. Phys. Chem. C 2017, 121, 16399−16414

(44) He, X. B.; Lyu, J. H.; Zhou, H.; Zhuang, G. L.; Zhong, X.; Wang, J. G.; Li, X. N. Density Functional Theory Study of *p*-Chloroaniline Adsorption on Pd Surfaces and Clusters. *Int. J. Quantum Chem.* **2014**, *114*, 895−899.
(45) Orita, H.; Nakamura, I.; Fujitani, T. A Density Functional Study of NO Adsorption and Decomposition on Ni(211) and Pd(211) Surfaces. *J. Chem. Phys.* **2005**, *122*, 014703.
(46) Kresse, G.; Furthmüller, J. Efficiency of Ab-Initio Total Energy Calculations for Metals and Semiconductors Using a Plane-Wave Basis Set. *Comput. Mater. Sci.* **1996**, *6*, 15−50.
(47) Perdew, J. P.; Burke, K.; Ernzerhof, M. Generalized Gradient Approximation Made Simple. *Phys. Rev. Lett.* **1996**, *77* (18), 3865−3868.
(48) Kresse, G.; Joubert, D. From Ultrasoft Pseudopotentials to the Projector Augmented-Wave Method. *Phys. Rev. B: Condens. Matter Mater. Phys.* **1999**, *59*, 1758−1775.
(49) Blöchl, P. E. Projector Augmented-Wave Method. *Phys. Rev. B: Condens. Matter Mater. Phys.* **1994**, *50*, 17953−17979.
(50) Jiang, Z.; Pan, Q.; Li, M. M.; Yan, T.; Fang, T. Density Functional Theory Study on Direct Catalytic Decomposition of Ammonia on Pd(111) Surface. *Appl. Surf. Sci.* **2014**, *292*, 494−499.
(51) Jiang, Z.; Qin, P.; Fang, T. Investigation on Adsorption and Decomposition of H_2S on Pd(100) Surface: A DFT Study. *Surf. Sci.* **2015**, *632*, 195−200.
(52) Henkelman, G.; Uberuaga, B. P.; Jónsson, H. A Climbing Image Nudged Elastic Band Method for Finding Saddle Points and Minimum Energy Paths. *J. Chem. Phys.* **2000**, *113*, 9901−9904.
(53) Henkelman, G.; Jónsson, H. Improved Tangent Estimate in the Nudged Elastic Band Method for Finding Minimum Energy Paths and Saddle Points. *J. Chem. Phys.* **2000**, *113*, 9978−9985.
(54) Lu, J. M.; Behtash, S.; Faheem, M.; Heyden, A. Microkinetic Modeling of the Decarboxylation and Decarbonylation of Propanoic Acid over Pd(111) Model Surfaces Based on Parameters Obtained from First Principles. *J. Catal.* **2013**, *305*, 56−66.
(55) Wang, J. B.; Sun, Q.; Chan, S.; Su, H. B. The Acceleration of Methanol Synthesis and C_2 Oxygenates Formation on Copper Grain Boundary from Syngas. *Appl. Catal., A* **2016**, *509*, 97−104.
(56) Hibbitts, D.; Neurock, M. Promotional Effects of Chemisorbed Oxygen and Hydroxide in the Activation C-H and O-H bonds over Transition Metal Surfaces. *Surf. Sci.* **2016**, *650*, 210−220.
(57) Li, F. X.; Luo, S. W.; Sun, Z. C.; Bao, X. G.; Fan, L. S. Role of Metal Oxide Support in Redox Reactions of Iron Oxide for Chemical Looping Applications: Experiments and Density Functional Theory Calculations. *Energy Environ. Sci.* **2011**, *4*, 3661−3667.
(58) Cheng, Z.; Fine, N. A.; Lo, C. S. Platinum Nanoclusters Exhibit Enhanced Catalytic Activity for Methane Dehydrogenation. *Top. Catal.* **2012**, *55*, 345−352.
(59) Zhang, R. G.; Guo, X. Q.; Wang, B. J.; Ling, L. X. Insight Into the Effect of CuNi(111) and FeNi(111) Surface Structure and Second Metal Composition on Surface Carbon Elimination by O or OH: A Comparison Study with Ni(111) Surface. *J. Phys. Chem. C* **2015**, *119*, 14135−14144.
(60) Gao, Q.; Ramsier, R. D.; Waltenburg, H. N.; Yates, J. T., Jr Unusual Adsorption Site Occupation Sequence: NO Adsorption on Stepped Pd(112). *J. Am. Chem. Soc.* **1994**, *116*, 3901−3903.
(61) Zeng, Z. H.; Da Silva, J. L. F.; Li, W. X. Density Functional Theory and Ab Initio Molecular Dynamics Study of NO Adsorption on Pd(111) and Pt(111) Surfaces. *Phys. Rev. B: Condens. Matter Mater. Phys.* **2010**, *81*, 085408.
(62) Dinerman, C. E.; Ewing, G. E. Infrared Spectrum, Structure, and Heat of Formation of Gaseous $(NO)_2$. *J. Chem. Phys.* **1970**, *53*, 626−631.
(63) Brown, W. A.; King, D. A. NO Chemisorption and Reactions on Metal Surfaces: A New Perspective. *J. Phys. Chem. B* **2000**, *104*, 2578−2595.
(64) Liu, Z. P.; Jenkins, S. J.; King, D. A. Why Is Silver Catalytically Active for NO Reduction? A Unique Pathway via an Inverted $(NO)_2$ Dimer. *J. Am. Chem. Soc.* **2004**, *126*, 7336−7340.
(65) Kim, C. M.; Yi, C. W.; Goodman, D. W. Adsorption and Reaction of NO on Cu(100): An Infrared Reflection Absorption Spectroscopic Study at 25 K. *J. Phys. Chem. B* **2002**, *106*, 7065−7068.
(66) Dumas, P.; Suhren, M.; Chabal, Y. J.; Hirschmugl, C. J.; Williams, G. P. Adsorption and Reactivity of NO on Cu(111): A Synchrotron Infrared Reflection Absorption Spectroscopic Study. *Surf. Sci.* **1997**, *371*, 200−212.
(67) Chen, Y.; Liu, Y. J.; Wang, H. X.; Zhao, J. X.; Cai, Q. H.; Wang, X. Z.; Ding, Y. H. Silicon-Doped Graphene: An Effective and Metal-Free Catalyst for NO Reduction to N_2O? *ACS Appl. Mater. Interfaces* **2013**, *5*, 5994−6000.
(68) Ferullo, R. M.; Fuente, S. A.; Branda, M. M.; Castellani, N. J. Theoretical Study of N_2O_2 Interaction with BaO(100) Surface. *J. Mol. Struct.: THEOCHEM* **2007**, *818*, 57−64.
(69) Luo, Q. Q.; Wang, T.; Beller, M.; Jiao, H. Hydrogen Generation from Formic Acid Decomposition on Ni(211), Pd(211) and Pt(211). *J. Mol. Catal. A: Chem.* **2013**, *379*, 169−177.
(70) Hao, X. B.; Wang, B. J.; Wang, Q.; Zhang, R. G.; Li, D. B. Insight into Both Coverage and Surface Structure Dependent CO Adsorption and Activation on Different Ni Surface from DFT and Atomistic Thermodynamics. *Phys. Chem. Chem. Phys.* **2016**, *18*, 17606−17618.
(71) Kling, Å.; Andersson, C.; Myringer, Å.; Eskilsson, D.; Järås, S. G. Alkali Deactivation of High-dust SCR Catalysts used for NO_x Reduction Exposed to Flue Gas from 100 MW-Scale Biofuel and Peat Fired Boilers: Influence of Flue Gas Composition. *Appl. Catal., B* **2007**, *69*, 240−251.
(72) Li, H. X.; Cormier, W. E; Moden, B. Novel Metal-Containing Zeolite Beta for NOx Reduction and Methods of Making the Same: U.S. Patent Application 13/110,337[P]. 2011.11.24.
(73) Li, H. X.; Cormier, W. E.; Moden, B. Iron-containing Aluminosilicate Zeolites and Methods of Making and Using Same: U.S. Patent 8,541,331[P]. 2013.9.24.
(74) Uchida, M.; Bell, A. T. A Study of NO Reduction by H_2 over an Alumina-Supported Ruthenium Catalyst. *J. Catal.* **1979**, *60*, 204−215.
(75) Wind, T. L.; Falsig, H.; Sehested, J.; Moses, P. G.; Nguyen, T. T. M. Comparison of Mechanistic Understanding and Experiments for CO Methanation over Nickel. *J. Catal.* **2016**, *342*, 105−116.
(76) Dhainaut, F.; Pietrzyk, S.; Granger, P. Kinetics of the NO+H_2 Reaction over Supported Noble Metal Based Catalysts: Support Effect on Their Adsorption Properties. *Appl. Catal., B* **2007**, *70*, 100−110.
(77) Matsushima, T. Surface Structural Information Carried by Desorbing Reaction Products. *Prog. Surf. Sci.* **2007**, *82*, 435−477.
(78) Haq, S.; Hodgson, A. N_2O Adsorption and Reaction at Pd(110). *Surf. Sci.* **2000**, *463*, 1−10.
(79) Matsushima, T.; Kokalj, A. N_2 Emission via Intermediate N_2O in a Steady-State NO + CO + D_2 Reaction on Stepped Pd(211) by Angle-Resolved Desorption. *J. Phys. Chem. C* **2015**, *119*, 11699−11713.
(80) Avery, N. R. An EELS Study of N_2O Adsorption on Pt(111). *Surf. Sci.* **1983**, *131*, 501−510.
(81) Li, Y. X.; Bowker, M. The Adsorption and Decomposition of Nitrous Oxide on Rh(110) and Rh(111). *Surf. Sci.* **1996**, *348*, 67−76.
(82) Väterlein, P.; Krause, T.; Bäßler, M.; Fink, R.; Umbach, E.; Taborski, J.; Wüstenhagen, V.; Wurth, W. Adsorption-Induced Bending of a Triatomic Molecule: Near-Edge X-Ray Absorption Fine Structure Spectroscopy Investigation of N_2O Adsorbed on Different Ni(111) Surfaces. *Phys. Rev. Lett.* **1996**, *76*, 4749−4752.
(83) Carré, S.; Dujardin, C.; Granger, P. Operando Infrared Spectroscopy of the Reduction of NO by H_2 over Rhodium Based Catalysts. *Catal. Today* **2012**, *191*, 59−64.
(84) Kondo, T.; Sakurai, M.; Matsushima, T.; Nakamura, J. Angle Resolved Intensity and Velocity Distributions of N_2 Desorbed by Decomposition on Rh(110). *J. Chem. Phys.* **2010**, *132*, 134704.
(85) Orita, H.; Kubo, T.; Matsushima, T.; Kokalj, A. DFT Calculations of Adsorption and Decomposition of N_2O on Rh(100). *J. Phys. Chem. C* **2010**, *114*, 21444−21449.
(86) Choi, Y. M.; Liu, P. Mechanism of Ethanol Synthesis from Syngas on Rh(111). *J. Am. Chem. Soc.* **2009**, *131* (36), 13054−13061.
(87) Zuo, Z. J.; Peng, F.; Huang, W. Efficient Synthesis of Ethanol from CH_4 and Syngas on a Cu-Co/TiO_2 Catalyst Using a Stepwise Reactor. *Sci. Rep.* **2016**, *6*, 34670.

DOI: 10.1021/acs.jpcc.7b05024
J. Phys. Chem. C 2017, 121, 16399−16414

(88) Fu, X. C.; Shen, W. X.; Yao, W. Y.; Hou, W. H. *Physical Chemistry*, 5th ed.; Higher Education Press,: Beijing, 2009; Vol. *2*, pp 235−244.
(89) Huang, L. F.; Ni, M. Y.; Zheng, X. H.; Zhou, W. H.; Li, Y. G.; Zeng, Z. Ab Initio Simulations of the Kinetic Properties of the Hydrogen Monomer on Graphene. *J. Phys. Chem. C* **2010**, *114* (51), 22636−22643.
(90) http://webbook.nist.gov/chemistry/.
(91) Fu, X. C.; Shen, W. X.; Yao, W. Y.; Hou, W. H. *Physical Chemistry* 5th; Higher Education Press: Beijing, 2009; Vol. *2*, pp 160−162.
(92) Hecker, W. C.; Bell, A. T. Reduction of NO by H_2 over Silica-Supported Rhodium: Infrared and Kinetic Studies. *J. Catal.* **1985**, *92*, 247−259.

DOI: 10.1021/acs.jpcc.7b05024
J. Phys. Chem. C 2017, 121, 16399−16414